Coordination Chemistry Reviews, 87 (1988) 1–54
Elsevier Science Publishers B.V., Amsterdam – Printed in The Netherlands

ELECTROCHEMISTRY OF METAL–SULFUR CLUSTERS: STEREOCHEMICAL CONSEQUENCES OF THERMODYNAMICALLY CHARACTERIZED REDOX CHANGES

Part II. Heterometal clusters

PIERO ZANELLO

Dipartimento di Chimica dell'Università di Siena, Pian dei Mantellini, 44-53100 Siena (Italy)

(Received 24 June 1987)

CONTENTS

0010-8545/88/$18.90

ABBREVIATIONS FOR SOLVENTS

AC acetone
AN acetonitrile
DCE 1,2-dichloroethane

DCM dichloromethane
DMA *N,N*-dimethylacetamide
DMF *N,N*-dimethylformamide
DMSO dimethylsulfoxide

A. INTRODUCTION

The interest in heterometal–sulfur clusters stems largely from the similarity between the physico-chemical properties of some Mo–Fe–S derivatives and those of the iron–molybdenum proteins (specifically the iron–molybdenum cofactor) of the nitrogenase enzyme [1–4]. In addition, the recent isolation of vanadium–iron proteins [5,6], probably also having a vanadium–iron cofactor [7], opens new fields to heterometallic clusters in molecular biology. Moreover, there is evidence that the involvement of heterometal–sulfur derivatives in biological functions is a more extended phenomenon [8,9].

Finally, equally significant goals appear in the use of heterometallic sulfur clusters as new catalytic materials [10].

As discussed in Part I of this review [11], in which the electrochemistry of metal–sulfur clusters is examined, here I will report (unless otherwise specified) electrode potentials with reference to the ferrocene/ferrocenium couple, in order to compare potentials from different solvents and from different reference electrodes. Dinuclear complexes are not included in the discussion.

B. HETERODIMETALLIC SULFUR CLUSTERS

Most of the currently known heterometallic sulfur clusters which have been electrochemically characterized belong to the class of dimetallic derivatives.

(i) Iron–cobalt clusters

(a) $FeCo_2S$ core

As discussed in Part I of this review (Section B (i)), the mixed metal cluster $FeCo_2S(CO)_9$ affords the opportunity to evaluate the structural consequences of the removal of the unpaired electron (residing in a strongly antibonding orbital) in $Co_3S(CO)_9$, $FeCo_2S(CO)_9$ being isoelectronic with $[Co_3S(CO)_9]^+$ [12]. Figure 1 shows the molecular structure of $FeCo_2S(CO)_9$. It consists of an equilateral metal triangle capped by an apical triply bridging sulfur atom, giving rise to an averaged structure of $C_{3v} - 3m$ geometry [12].

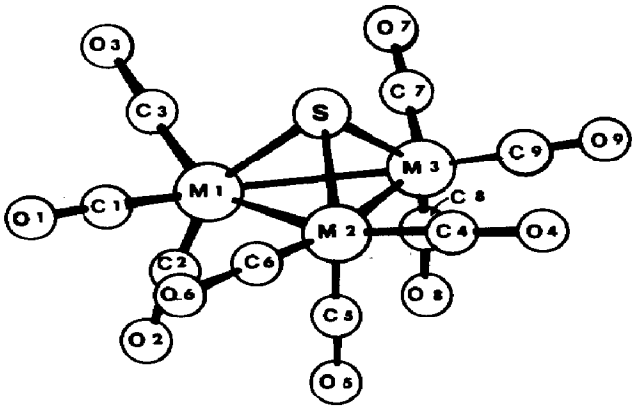

Fig. 1. Molecular structure of $FeCo_2S(CO)_9$ (from ref. 12).

The electrode behavior of $FeCo_2S(CO)_9$ in different solvents clearly indicates its ability to be reversibly, or near reversibly, reduced to the radical anion $[FeCo_2S(CO)_9]^-$ [13,14]. Since this monoanion has a half-life of about 1 min at room temperature, the appearance of further reduction steps has been attributed to fragmentation products. It has also been hypothesized that the heterogeneous electron transfer occurs via the apical sulfur atom [13]. Table 1 reports the redox potentials for the charge transfer $0/1-$.

Assuming the anion $[FeCo_2S(CO)_9]^-$ to be equivalent to $Co_3S(CO)_9$, the addition of one electron to $FeCo_2S(CO)_9$ causes a significant elongation of the average metal–metal distances from 2.55 to 2.64 Å, and a slight shortening of the average metal–sulfur distances from 2.16 to 2.14 Å [12]. These data agree with the view that the electron enters an antibonding orbital, essentially metallic in character [12,13].

As shown in Table 1, the gradual substitution of carbonyl groups with weaker π-acceptors such as aryl isocyanides [14] or triphenylphosphite [13], increasing the electronic density on the trimetallic core, makes the reduction step more and more difficult.

(b) Fe_2CoS core

On the basis of spectroscopic properties, a triangular pyramidal structure similar to that of $FeCo_2S(CO)_9$ was proposed for the $[Fe_2CoS(CO)_9]^-$ anion [15]. In 1,2-dichloroethane this monoanion undergoes both a quasi-reversible one-electron oxidation and a quasi-reversible one-electron reduction [14] according to the following sequence:

$$Fe_2CoS(CO)_9 \underset{-e^-}{\overset{+e^-}{\rightleftarrows}} [Fe_2CoS(CO)_9]^- \underset{-e^-}{\overset{+e^-}{\rightleftarrows}} [Fe_2CoS(CO)_9]^{2-}$$

$$E^{\circ\prime} = +0.16\ \text{V} \qquad E^{\circ\prime} = -2.12\ \text{V}$$

TABLE 1

Formal electrode potentials (in volts) for the reduction processes of $FeCo_2S(CO)_{9-n}L_n$

L	n	Redox change 0/1−	Solvent	Ref.
–	0	−0.80	AC	13
–	0	−1.09	DCE	14
$P(OC_6H_5)_3$	1	−1.42	AC	13
CH_3O-*p*-C_6H_4NC	1	−1.36	DCE	14
CH_3-*p*-C_6H_4NC	1	−1.35	DCE	14
CH_3-*o*-C_6H_4NC	1	−1.32	DCE	14
CH_3-*m*-C_6H_4NC	1	−1.33	DCE	14
C_6H_5NC	1	−1.33	DCE	14
Cl-*o*-C_6H_4NC	1	−1.30	DCE	14
$C_6H_5CH_2NC$	1	−1.34	DCE	14
NO_2-*p*-C_6H_4NC	1	−1.28	DCE	14
CH_3O-*p*-C_6H_4NC	2	−1.57	DCE	14
CH_3-*p*-C_6H_4NC	2	−1.56	DCE	14
CH_3-*o*-C_6H_4NC	2	−1.53	DCE	14
CH_3-*m*-C_6H_4NC	2	−1.54	DCE	14
C_6H_5NC	2	−1.53	DCE	14
Cl-*o*-C_6H_4NC	2	−1.51	DCE	14
$C_6H_5CH_2NC$	2	−1.54	DCE	14
NO_2-*p*-C_6H_4NC	2	−1.47	DCE	14
CH_3O-*p*-C_6H_4NC	3	−1.86	DCE	14
CH_3-*p*-C_6H_4NC	3	−1.83	DCE	14
CH_3-*m*-C_6H_4NC	3	−1.80	DCE	14
C_6H_4NC	3	−1.78	DCE	14
Cl-*o*-C_6H_4NC	3	−1.73	DCE	14

Diagnostic parameters indicate that the dianion is a stable product, while the neutral species is stable only for a short time.

Since $[Fe_2CoS(CO)_9]^-$ is isoelectronic with $FeCo_2S(CO)_9$, the comparison between the relevant redox potentials for the addition of one electron clearly demonstrates that coulombic repulsions greatly destabilize the trimetal antibonding LUMO orbital of $[Fe_2CoS(CO)_9]^-$.

(ii) Iron–molybdenum clusters

In accordance with the two most likely models for the Fe–Mo–S clusters of nitrogenase [1–4], represented in Scheme 1, the synthetic approach to

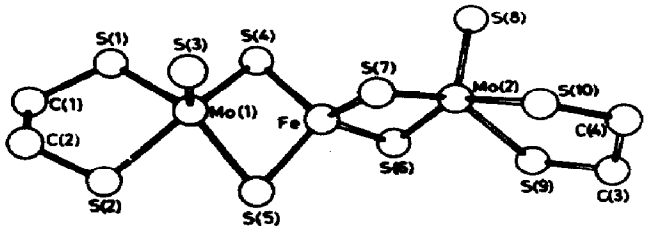

Fig. 2. Molecular geometry of $\{[(SCH_2CH_2S)MoS_3]_2Fe\}^{3-}$. Mean distances: Mo–Fe 2.75 Å; $Mo–S_{(terminal)}$ 2.14 Å; $Mo–S_{(bridging)}$ 2.32 Å; $Mo–S_{(mercapto)}$ 2.40 Å; Fe–S 2.22 Å; Mo–$\widehat{Fe}$-Mo 155.7° (from ref. 16).

iron–molybdenum clusters has followed both the "cubane" heterometallic assembly and the "linear" heterometallic assembly.

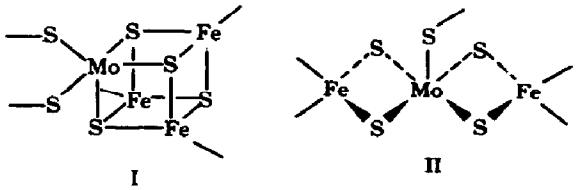

I II

Scheme 1

(a) $FeMo_2S_4$ core

See Appendix.

(b) $FeMo_2S_6$ core

The molecular structure of the trianion $\{[(SCH_2CH_2S)MoS_3]_2Fe\}^{3-}$ is shown in Fig. 2 [16].

The anion contains a central tetrahedrally coordinated Fe(III) atom and two pseudotetragonal–pyramidal Mo(V) atoms.

In acetonitrile solution, $\{[(SCH_2CH_2S)MoS_3]_2Fe\}^{3-}$ undergoes a quasi-reversible one-electron reduction ($E°' = -1.05$ V), followed at more negative potentials (~ -1.9 V) by a multielectron process [16]. No information is available as far as the stability and/or structure of the tetra-anion is concerned.

(c) $FeMo_2S_8$ core

The trianion $[(MoS_4)_2Fe]^{3-}$ was independently prepared by two groups [17,18]. Figure 3 shows its molecular structure [18] to consist of a central tetrahedrally coordinated Fe atom bound by two tetrathiomolybdate anions. Recent studies formulate it as an iron(I) complex coordinated by two diamagnetic $Mo^{VI}S_4$ anions [19].

The trianion undergoes, in acetonitrile solvent, a quasi-reversible one-electron reduction (3 − /4 −) ($E°' = -2.12$ V) and an irreversible one-electron oxidation (3 − /2 −) ($E_p = -0.30$ V) (Fig. 4) [17].

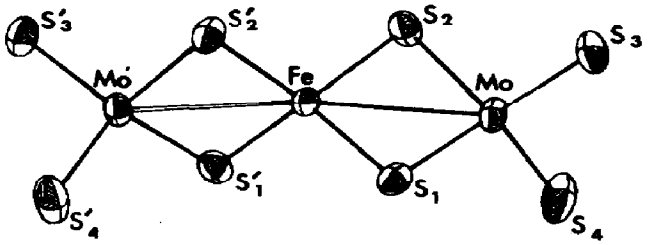

Fig. 3. Perspective view of $[(MoS_4)_2Fe]^{3-}$. Mean distances: Mo–Fe 2.74 Å; $Mo–S_{(terminal)}$ 2.17 Å; $Mo–S_{(bridging)}$ 2.26 Å; Fe–S 2.26 Å; Mo–$\widehat{Fe}$–Mo 172.6° (from ref. 18).

The irreversibility of the $3-/2-$ step renders the existence of the dianion $[Fe(MOS_4)_2]^{2-}$ uncertain [20].

(d) Fe_2MoS_4 core

The dianion $[(FeCl_2)_2MoS_4]^{2-}$ has recently been prepared and characterized [21,22]. It consists of a central tetrahedral tetrathiomolybdate anion bridging two $FeCl_2$ units (Fig. 5).

In dichloromethane, $[Cl_2FeS_2MoS_2FeCl_2]^{2-}$ undergoes a quasi-reversible one-electron reduction $(2-/3-)$ coupled with following chemical complications (identified as a loss of chloride ion from the unstable $[Cl_2FeS_2MoS_2FeCl_2]^{3-}$) leading to $[(MoS_4)Fe_2Cl_3]^{2-}$. Similar behavior oc-

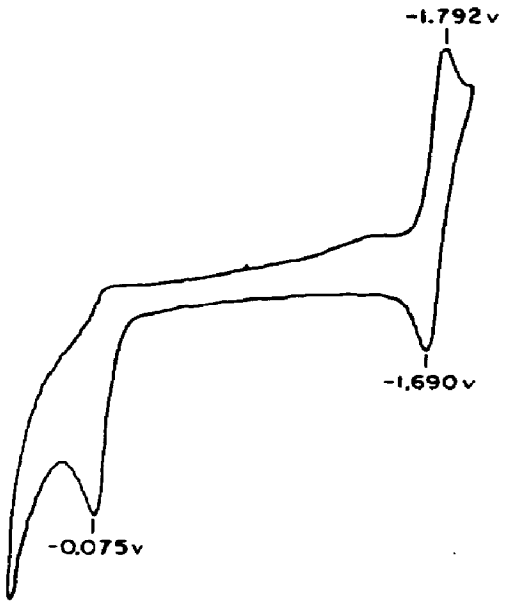

Fig. 4. Cyclic voltammetric behavior of $[Fe(MoS_4)_2]^{3-}$ in acetonitrile solution. Potential values vs. SCE (from ref. 17).

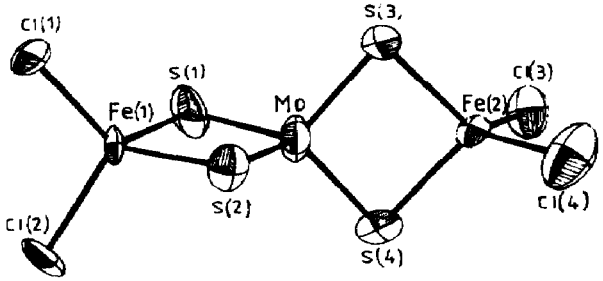

Fig. 5. Molecular structure of $[Cl_2FeS_2MoS_2FeCl_2]^{2-}$. Mean distances: Mo–Fe 2.78 Å; Fe–S 2.30 Å; Mo–S 2.21 Å; Fe–Cl 2.23 Å; Fe–$\widehat{Mo}$–Fe 179.4° (from ref. 21).

curs with $[Br_2FeS_2MoS_2FeBr_2]^{2-}$ [22]. Table 2 reports the redox potentials for the $[X_2FeS_2MoS_2FeX_2]^{2-/3-}$ couples (X = Cl, Br).

(e) Fe_2MoS_6 core

One further component of the "linear" heterometallic trinuclear sulfur derivatives is the trianion $[(C_6H_5S)_2FeS_2FeS_2MoS_2]^{3-}$ (Fig. 6) [23]. The presence of Fe atoms in two distinct sites should be noted. The trianion undergoes (in acetonitrile?) both an irreversible oxidation at +0.3 V and an irreversible reduction at −1.4 V [23], clearly indicating it to be the only stable member of the trinuclear Fe–Fe–Mo sulfur clusters.

(f) $Fe_2Mo_2S_3$ core

See Appendix.

(g) $Fe_2Mo_2S_4$ core

See Appendix.

(h) Fe_3MoS_4 core

As seen in Scheme 1, the iron–molybdenum cubane clusters are important models for nitrogenases. A wide series of "single-cubane" Fe_3MoS_4 clusters has been characterized, and their reactivity (Scheme 2) fully demonstrated [24]. The synthesis of the precursors (type **1**) begins with the solvent-induced cleavage of bridged "double-cubane" iron–molybdenum clusters [25–27],

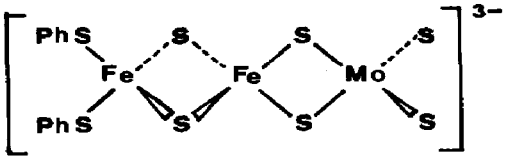

Fig. 6. Proposed structure for $[(C_6H_5S)_2FeS_2FeS_2MoS_2]^{3-}$.

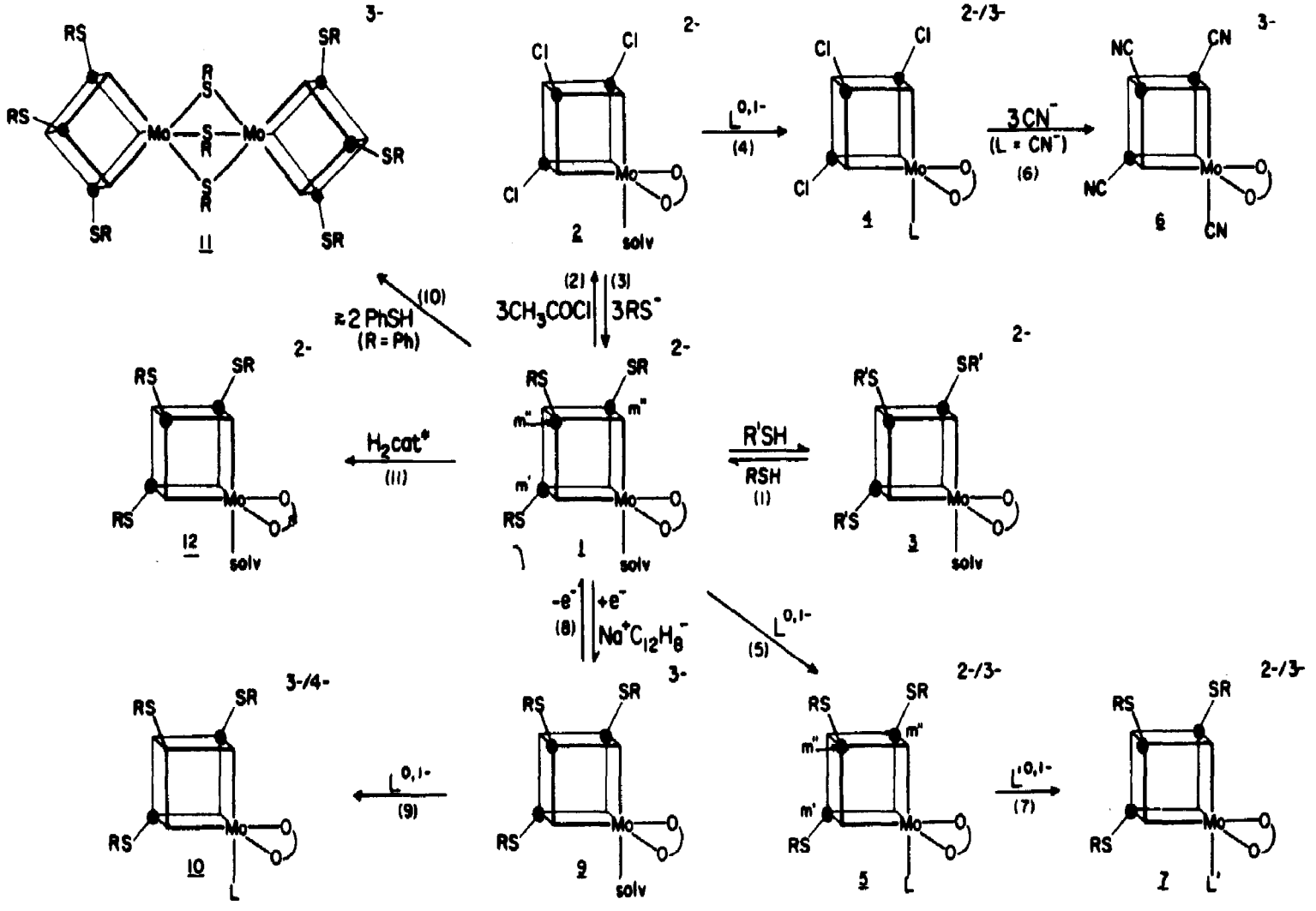
3-
RS
SR
Mo
S
R
11
2-
Cl
2
solv
L 0,1-
(4)
2-/3-
4
L
3CN⁻
(L = CN⁻)
(6)
NC
CN
6
(10)
≥2 PhSH
(R = Ph)
(2)
(3)
3CH3COCl
3RS⁻
12
H2cat⁴⁻
(11)
1
m''
m'
R'SH
RSH
(1)
R'S
SR'
3
-e⁻
+e⁻
(8)
Na⁺C12H8⁻
L 0,1-
(5)
3-/4-
10
L 0,1-
(9)
9
5
L 0,1-
(7)
7
L'
● Fe
L,L' = generic ligands
O O = catecholate

Scheme 2

TABLE 2

Approximate [a] standard potentials (in volts) for the 2−/3− couple of $[X_2FeS_2MoS_2FeX_2]^{2-}$ (X = Cl, Br) in dichloromethane solvent [21,22]

X	$E^{\circ\prime}$
Cl	−1.04
Br	−1.02

[a] Calculated from cyclic voltammetric responses at $i_{pa}/i_{pc} = 0.7$, where i_{pa} and i_{pc} are the anodic and cathodic peak current respectively. In order to obtain a thermodynamic value an i_{pa}/i_{pc} ratio equal to unity would be required.

which we shall examine later (Sections B (ii) (k)–(o)). The solvated clusters **1** are stable in solution, but cannot be obtained in the crystalline form because they revert to the corresponding double-cubane species. These clusters, which have a $[MoFe_3S_4]^{3+}$ core, undergo both a quasi-reversible one-electron oxidation and a quasi-reversible one-electron reduction [26,27], according to the following three-membered series:

$$[MoFe_3S_4]^{4+} \underset{-e^-}{\overset{+e^-}{\rightleftarrows}} [MoFe_3S_4]^{3+} \underset{-e^-}{\overset{+e^-}{\rightleftarrows}} [MoFe_3S_4]^{2+}$$

Table 3 shows the redox potentials of a number of these single-cubane solvated derivatives.

The difference between the standard potentials of the two redox changes (0.9–1.0 eV) may constitute a good measure of the difference in energy between the HOMO–LUMO of the $[MoFe_3S_4]^{3+}$ core of these solvated species. (In fact, from the comparison in different solvents, the solvation terms seem unimportant.)

TABLE 3

Standard potentials (in volts) for the redox changes of a series of $[MoFe_3S_4(SR)_3(catecholate)(solvent)]^{2-}$ dianions

R	Catecholate	$E^{\circ\prime}_{2-/3-}$	$E^{\circ\prime}_{2-/1-}$	Solvent	Ref.
C_2H_5	3,6-(*n*-$C_3H_7)_2C_6H_2O_2$	−1.78	–	DMSO	26
C_2H_5	3,6-$(C_3H_5)_2C_6H_2O_2$	−1.78	−0.80	DMSO	26,27
C_6H_5	3,6-$(C_3H_5)_2C_6H_2O_2$	−1.58	–	DMSO	26
Cl-*p*-C_6H_4	3,6-$(C_3H_5)_2C_6H_2O_2$	−1.53	−0.56 [a]	DMSO	26,27
Cl-*p*-C_6H_4	3,6-$(C_3H_5)_2C_6H_2O_2$	−1.57	−0.65	DMF	27
Cl-*p*-C_6H_4	3,6-$(C_3H_5)_2C_6H_2O_2$	−1.40	−0.46	AN	27
CH_3-*p*-C_6H_4	3,6-(*n*-$C_3H_7)_2C_6H_2O_2$	−1.62	–	DMSO	26

[a] Peak potential value for irreversible processes.

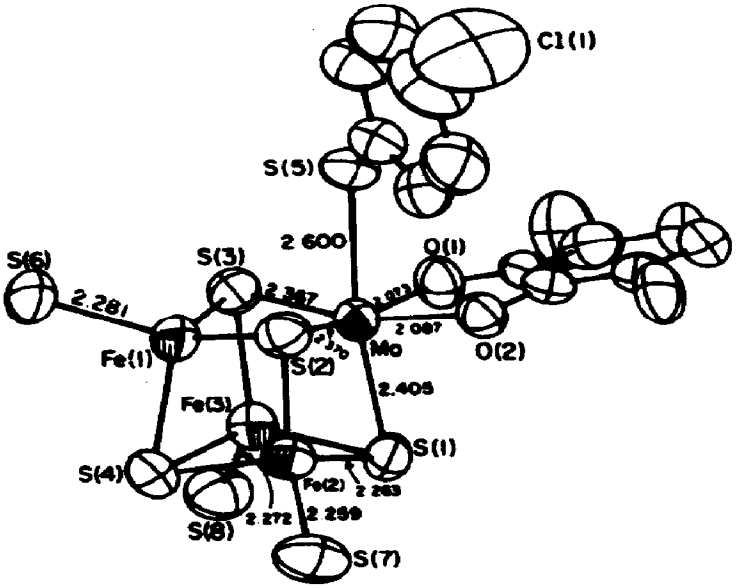

Fig. 7. Crystal structure of $[MoFe_3S_4(SC_6H_4\text{-}p\text{-}Cl)_4\{3,6\text{-}(C_3H_5)_2C_6H_2O_2\}]^{3-}$. Core mean distances: Fe–S 2.27 Å; Mo–S 2.38 Å; Fe · · · Fe 2.69 Å; S · · · S 3.65 Å (from ref. 25).

The one-electron reduction can also be achieved by chemical reductants (sodium acenaphthylenide). In this manner the reduced species $[MoFe_3S_4(S\text{–}C_6H_4\text{-}p\text{-}Cl)_3\{3,6\text{-}(C_3H_5)_2C_6H_2O_2\}(C_2H_5CN)]^{3-}$ (a derivative of type **9** in Scheme 2) has been obtained and spectroscopically characterized [28].

Precursors **1** can easily be converted to the ligated derivatives **5** [25–27]. Figure 7 shows the molecular structure of $[MoFe_3S_4(S\text{–}C_6H_4\text{-}p\text{-}Cl)_4\{3,6\text{-}(C_3H_5)_2C_6H_2O_2\}]^{3-}$ [25–27].

The cubane-like $MoFe_3S_4$ core is composed of two interpenetrating, imperfect $MoFe_3$ and S_4 tetrahedra giving rise to trigonal distortion from cubic symmetry. Each Fe atom occupies an approximately tetrahedral site, whereas the Mo atom is involved in distorted octahedral geometry.

The structures of $[Fe_3MoS_4(SC_2H_5)_3(Cl_4C_6O_2)(CN)]^{3-}$ and $[Fe_3MoS_4(SC_6H_4\text{-}p\text{-}Cl)_3(Cl_4C_6O_2)(N_3)]^{3-}$ have also been solved [24].

Like the solvated clusters, the ligated clusters **5** undergo both a quasi-reversible one-electron oxidation and a quasi-reversible one-electron reduction [25,27] (Fig. 8). Table 4 summarizes the redox potentials for the charge transfers involving clusters **5**.

Once again we can compute a value of about 1.0 eV for the HOMO–LUMO difference in energy for the $[Fe_3MoS_4]^{3+}$ core of these ligated cubane derivatives.

The thiolate groups of precursor **1** can readily be substituted by electrophilic moieties such as chloride to give compounds of type **2**.

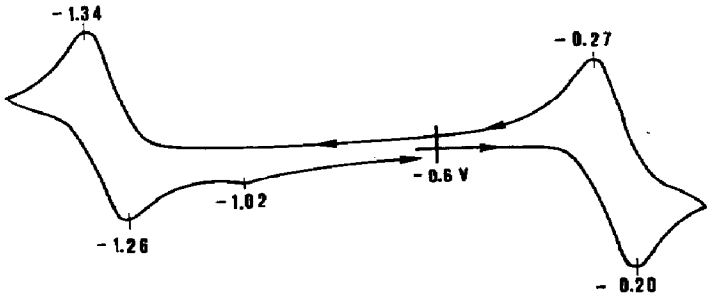

Fig. 8. Cyclic voltammogram recorded in an acetonitrile solution of $[MoFe_3S_4(SC_6H_4\text{-}p\text{-}Cl)_3\{3,6\text{-}(C_3H_5)_2C_6H_2O_2\}CN]^{3-}$. Potential values vs. SCE (from ref. 25).

Figure 9 shows the structure of $[MoFe_3S_4Cl_3\{3,6\text{-}(C_3H_5)_2C_6H_2O_2\}(THF)]^{2-}$ (THF = tetrahydrofuran) [29]. The $[Fe_3MoS_4]^{3+}$ core is similar to that of $[Fe_3MoS_4(SC_6H_4\text{-}p\text{-}Cl)_4\{3,6\text{-}(C_3H_5)_2C_6H_2O_2\}]^{3-}$, except for a slight variation in volume (9.56 Å^3 in the tetrathiolate species, 9.37 Å^3 in the trichloride species), which reflects the different coordination to a polarizable anionic thiolate in comparison with a hard neutral THF ligand [29].

In acetonitrile, the most significant redox change is the following:

$$[MoFe_3S_4Cl_3\{3,6\text{-}(C_3H_5)_2C_6H_2O_2\}(solv)]^{2-} \rightleftarrows$$

$$E^{\circ\prime} = -1.40\ \text{V}$$

$$\overset{+e^-}{\underset{-e^-}{\rightleftarrows}} \quad [MoFe_3S_4Cl_3\{3,6\text{-}(C_3H_5)_2C_6H_2O_2\}(solv)]^{3-}$$

No attempt to isolate the apparently stable trianion seems to have been made.

Another set of derivatives containing an $[Fe_3MoS_4]^{3+}$ core has very recently been obtained using 1,2-bis(dimethylphosphino)ethane as a cleaving agent of Fe(III)-bridged double-cubane species (see Section B (ii) (o)) [30].

TABLE 4

Redox potentials (in volts) for the redox changes of $[MoFe_3S_4(SR)_3\{3,6\text{-}(C_3H_5)_2C_6H_2O_2\}L]^{n-}$ in acetonitrile [27]

R	L	n	$E^{\circ\prime}_{n-/(n+1)-}$	$E^{\circ\prime}_{n-/(n-1)-}$
Cl-p-C_6H_4	S-C_6H_4-p-Cl	3	−1.45	−0.74 [a]
Cl-p-C_6H_4	CN	3	−1.68	−0.62
C_2H_5	CN	3	−1.98	−0.92
Cl-p-C_6H_4	OC_6H_5	3	−1.48	−0.67 [a]
Cl-p-C_6H_4	$P(C_2H_5)_3$	2	−1.56	−0.51

[a] Peak potential values for irreversible processes.

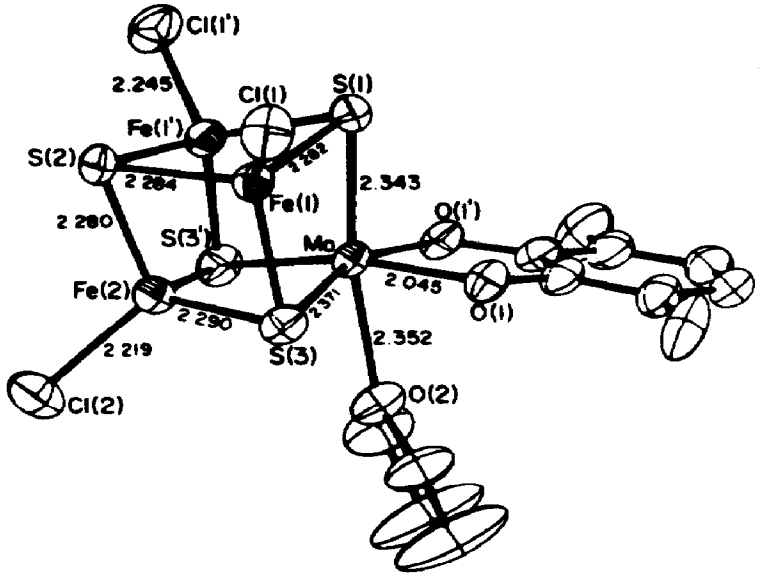

Fig. 9. Molecular structure of $[MoFe_3S_4Cl_3\{3,6\text{-}(C_3H_5)_2C_6H_2O_2\}(THF)]^{2-}$. Core mean distances: Fe–S 2.28 Å; Mo–S 2.36 Å; Fe · · · Fe 2.73 Å; S · · · S 3.62 Å (from ref. 29).

These single cubanes are of the type indicated in Scheme 3. With respect

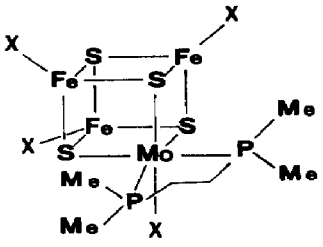

X = SC_2H_5, Cl

Scheme 3

to those preceding, the usual catecholate ligand is substituted by the

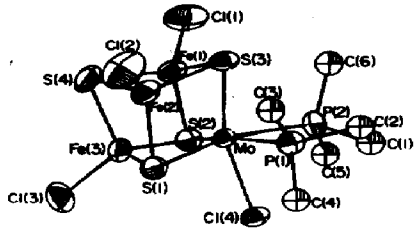

Fig. 10. Structure of $[MoFe_3S_4Cl_4(dpme)]^-$ (dmpe = 1,2-bis(dimethylphosphino)ethane). Core mean distances: Fe–S 2.27 Å; Mo–S 2.35 Å; Fe · · · Fe 2.75 Å; Mo · · · Fe 2.71 Å (from ref. 30).

bifunctional phosphine and all the metal centres have the same ligand. As an example, Fig. 10 shows the molecular structure of $\{MoFe_3S_4Cl_4[(CH_3)_2PCH_2CH_2P(CH_3)_2]\}^-$. The essential features of the cubane $[Fe_3MoS_4]^{3+}$ core parallel those described previously.

In this case also, the most significant redox change in acetonitrile solution is the reversible one-electron reduction:

$$[MoFe_3S_4(SC_2H_5)_4(dmpe)]^- \underset{-e^-}{\overset{+e^-}{\rightleftarrows}} [MoFe_3S_4(SC_2H_5)_4(dmpe)]^{2-} \qquad E^{\circ\prime} = -1.86\ V$$

$$[MoFe_3S_4Cl_4(dmpe)]^- \underset{-e}{\overset{+e^-}{\rightleftarrows}} [MoFe_3S_4Cl_4(dmpe)]^{2-} \qquad E^{\circ\prime} = -1.09\ V$$

Isolation of the one-electron reduced cluster has not yet been accomplished.

(i) Fe_4MoS_4 core

The first attempts to obtain single-cubane iron–molybdenum clusters from double-cubane clusters afforded the species $[Fe_4MoS_4(SC_2H_5)_3(C_6H_4O_2)_3]^{3-}$ [31].

The derivative is constructed of a cubane-like $MoFe_3S_4(SC_2H_5)_3$ unit bound to a tris-catecholate $Fe(C_6H_4O_2)_3$ subunit [31] (Fig. 11). The geometry and dimensions of the $MoFe_3S_4$ cube are closely related to those cited in Section B (ii) (h).

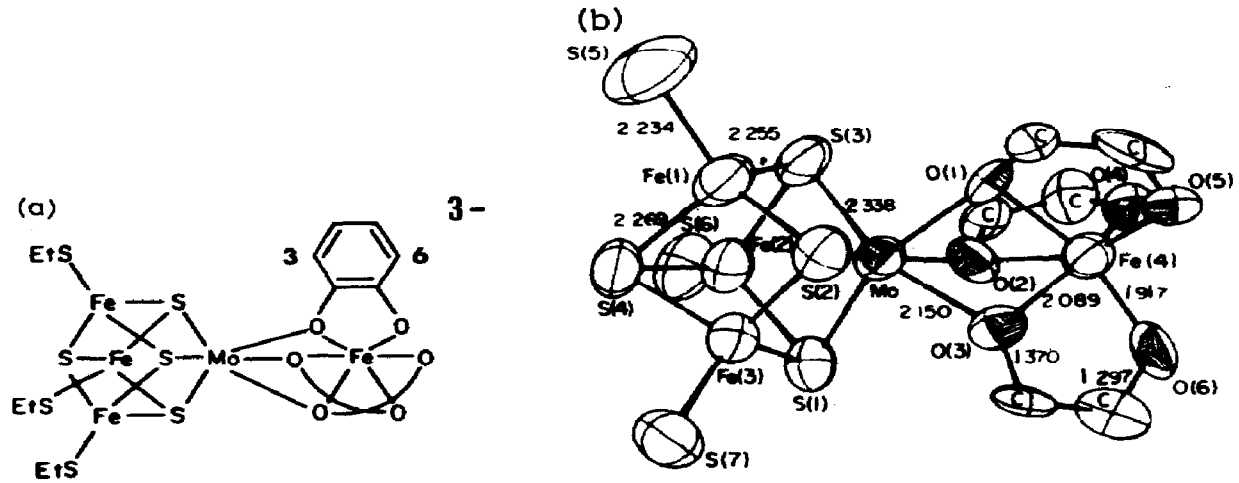

Fig. 11. Schematic representation (a) and molecular structure (b) of $[Fe_4MoS_4(SC_2H_5)_3(C_6H_4O_2)_3]^{3-}$. Mean distances in the Fe_3MoS_4 core: Fe–S 2.26 Å; Mo–S 2.34 Å; Fe · · · Fe 2.71 Å; S · · · S 3.60 Å (from ref. 31).

Figure 12 reports the cyclic voltammetric behavior of $[Fe_4MoS_4(SC_2H_5)_3(C_6H_4O_2)_3]^{3-}$ in acetonitrile solvent [31].

Both the anodic and the first cathodic process are attributable to the previously described sequence (see Section B (ii) (h)):

$$[MoFe_3S_4]^{4+} \underset{-e^-}{\overset{+e^-}{\rightleftarrows}} [MoFe_3S_4]^{3+} \qquad E^{\circ\prime} = -0.63 \text{ V}$$

$$[MoFe_3S_4]^{3+} \underset{-e^-}{\overset{+e^-}{\rightleftarrows}} [MoFe_3S_4]^{2+} \qquad E^{\circ\prime} = -1.69 \text{ V}$$

The constancy in the difference between the potential values of the two redox changes (about 1.0 V) for the $[MoFe_3S_4]^{3+}$ cores should be noted. The second irreversible cathodic process is attributed to the Fe(III)/Fe(II) reduction centered on the $Fe(C_6H_4O_2)_3$ subunit [31].

(j) $Fe_4Mo_4S_{20}$ core

The synthesis and properties of the $[Fe_4Mo_4S_{20}]^{6-}$ cluster have been reported [32]. On the basis of spectroscopic data, the researchers proposed a structure in which each Fe atom of a cubane-like Fe_4S_4 core is coordinated to an exogenous bidentate $[MoS_4]^{2-}$ ligand.

Indeed the stoicheiometry of the complex is doubtful, and it may simply be the $[Fe(MoS_4)_2]^{3-}$ trianion [18]. We note, however, that at least from the electrochemical behavior reported, some difference apparently exists; in fact, while $[Fe(MoS_4)_2]^{3-}$ undergoes (in acetonitrile) an irreversible one-electron oxidation ($E_p = -0.30$ V) and a quasi-reversible one-electron reduction ($E^{\circ\prime} = -2.12$ V) (see Section B (ii) (c)), $[Fe_4Mo_4S_{20}]^{6-}$ undergoes (in *N*,*N*-dimethylacetamide) an irreversible one-electron reduction ($E_p \sim -1.4$ V) and a further declustering multielectron reduction ($E_p \sim -2.0$ V) [32].

(k) $Fe_6Mo_2S_6$ core

Clusters containing an $Fe_6Mo_2S_6$ core have recently been characterized

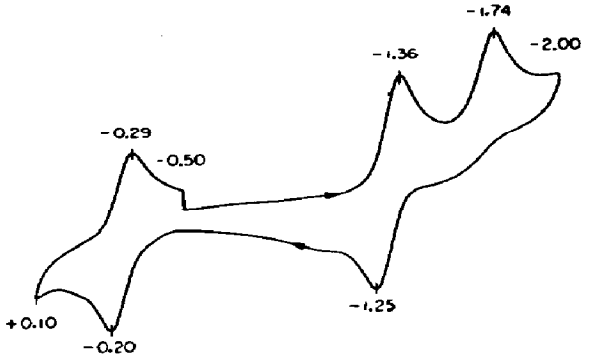

Fig. 12. Cyclic voltammogram recorded in an acetonitrile solution of $[Fe_4MoS_4(SC_2H_5)_3(C_6H_4O_2)_3]^{3-}$. Potential values vs. SCE (from ref. 31).

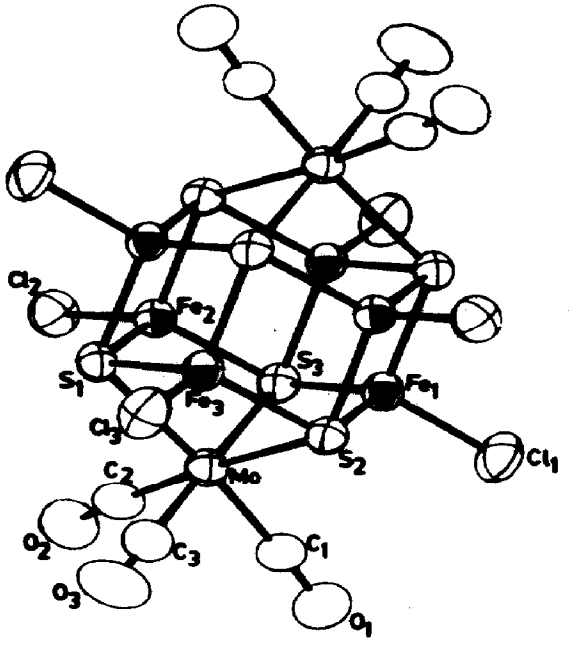

Fig. 13. Structure of the tetra-anion $[Fe_6S_6Cl_6\{Mo(CO)_3\}_2]^{4-}$ (from ref. 34).

[33,36]. Figure 13 shows the molecular structure of $[Fe_6S_6Cl_6\{Mo(CO)_3\}_2]^{4-}$.

The core can be thought of as a "prismane" $Fe_6S_6Cl_6$ unit (see Section B (vii)) in Part I of this review) bicapped by a $Mo(CO)_3$ unit. This addition essentially causes an elongation of the Fe_6S_6 central cage with respect to the original "prismane" core.

The most significant redox processes of these species are the two reversible one-electron steps $3-/4-$ and $4-/5-$ (Table 5).

Because of the chemical reversibility of these charge transfers, isolation of congeners of these clusters was possible. In fact, $[Fe_6S_6Cl_6(Mo(CO)_3)_2]^{3-}$ has been obtained and fully characterized [34,36]. The comparison between the structures of the tetra-anion (possessing an $[Fe_6Mo_2S_6]^{2+}$ core) and the corresponding trianion (possessing an $[Fe_6Mo_2S_6]^{3+}$ core) shows that the

TABLE 5

Redox potentials (in volts) for the redox processes of $[Fe_6S_6X_6\{Mo(CO)_3\}_2]^{n-}$

X	n	$E^{\circ\prime}_{3-/4-}$	$E^{\circ\prime}_{4-/5-}$	Solvent	Ref.
OC_6H_4-p-CH_3	3	−0.84	−1.38	DCM	33, 35
SC_6H_5	3	−0.83	−1.27	DCM	33
Cl	4	−0.43	−0.93	AN	34
Cl	3	−0.44	–	DCM	36
Br	3	−0.41	–	DCM	36

removal of one electron causes a shortening of both the Fe–Mo distance (from 3.00 to 2.93 Å) and the Mo–S distance (from 2.62 to 2.58 Å) in the bicapping units, while leaving practically untouched the interatomic distances within the central Fe_6S_6 unit [36]. This suggests that the HOMO of the tetra-anion, antibonding in character, mainly arises from Mo and S atomic orbitals [36].

(l) $Fe_6Mo_2S_8$ core

The "double-cubane" clusters constitute one of the first class of polynuclear iron–molybdenum–sulfur derivatives prepared and fully characterized.

Clusters containing an $Fe_6Mo_2S_8$ assembly are of the types represented in Scheme 4.

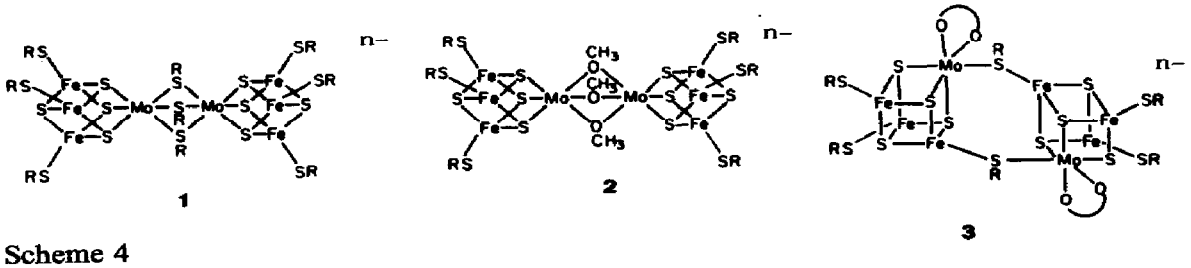

Scheme 4

Figure 14 shows the molecular structure of the trianion $[Fe_6Mo_2S_8(SC_6H_5)_9]^{3-}$ [37], which can be assumed representative of the triply bridged species $[Mo_2Fe_6S_8(\mu\text{-}SR)_3(SR)_6]^{3-}$ (**1**). The structures of the related trianions $[Fe_6Mo_2S_8(SCH_2CH_2OH)_9]^{3-}$ [38] and $[Fe_6Mo_2S_8(SC_2H_5)_9]^{3-}$ [39,44] have also been solved. The trianion is constructed of two Fe_3MoS_4 cubane-like units linked through the molybdenum atoms by three thiolate ligands.

These trianion clusters offer a wide range of one-electron transfer steps,

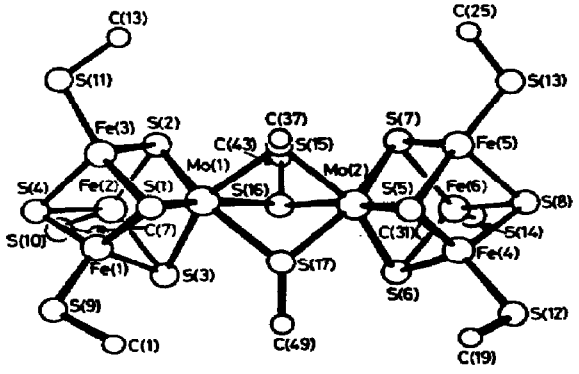

Fig. 14. Perspective view of $[Fe_6Mo_2S_8(SC_6H_5)_9]^{3-}$ (from ref. 37).

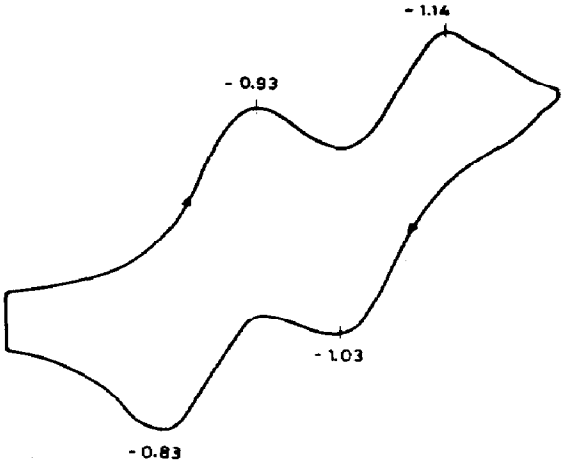

Fig. 15. Cyclic voltammogram recorded in a dimethylformamide solution of $[Fe_6Mo_2S_8(SC_6H_5)_9]^{3-}$ (from ref. 41).

depending upon the different substituents. The following sequence has been found [40]:

$$(2-)\xleftarrow[-e^-]{}(3-)\underset{-e^-}{\overset{+e^-}{\rightleftarrows}}(4-)\underset{-e^-}{\overset{+e^-}{\rightleftarrows}}(5-)\xrightarrow{+e^-}(6-)\xrightarrow{+e^-}(7-)$$

The $3-/4-$ and $4-/5-$ steps are the most significant redox processes for all complexes because of their chemical reversibility. As an example, Fig. 15 shows the cyclic voltammetric behavior of $[Fe_6Mo_2S_8(SC_6H_5)_9]^{3-}$ in the potential range useful for the occurrence of the two successive reduction steps $3-/4-$ and $4-/5-$. It is commonly accepted that these two sequentially added electrons separately enter each of the two Fe_3MoS_4 halves [40,42], according to the following sequence [42]:

$$[Ox\text{–}Ox]^{3-}\underset{-e^-}{\overset{+e^-}{\rightleftarrows}}[Ox\text{–}Red]^{4-}\underset{-e^-}{\overset{+e^-}{\rightleftarrows}}[Red\text{–}Red]^{5-}$$

If the two cubane units were non-interacting, then on the basis of a well-known treatment [43], a difference of 0.036 V is expected between the standard potentials of the two (quasi-reversible) charge-transfers. Indeed, as can be deduced from Table 6, this difference is generally higher (~ 0.2 V), indicating that each site influences to some extent the other during the reduction, although the intersite distance is about 3.7 Å [42].

The chemical reversibility of the $3-/4-$ and $4-/5-$ redox processes allows one to electrogenerate both the tetra-anion and penta-anion forms of the $Fe_6Mo_2S_8$ core. Both the congeners $[Fe_6Mo_2S_8(SC_6H_5)_9]^{4-,5-}$ of $[Fe_6Mo_2S_8(SC_6H_5)_9]^{3-}$ have been obtained [45]. While the tetra-anion has been spectroscopically characterized, the penta-anion has also been char-

TABLE 6

Standard electrode potentials (in volts) for the reduction processes of $[Fe_6Mo_2S_8(\mu\text{-}SR)_3(X)_6]^{3-}$

R	X	$E^{\circ\prime}_{3-/4-}$	$E^{\circ\prime}_{4-/5-}$	Solvent	Ref.
C_2H_5	SC_2H_5	−1.66	−1.85	AN	44,48
C_2H_5	SC_2H_5	−1.67	−1.87	DMSO	39,45,46
C_2H_5	SC_2H_5	−1.77	−1.98	DMF	45
C_2H_5	SCH_2CH_2OH	−1.67	−1.87	DMF	45
C_2H_5	SC_6H_5	−1.39	−1.57	AN	48
C_2H_5	Cl	−1.21	−1.39	AN	50 [a]
C_2H_5	Br	−1.17	−1.37	AN	40
C_2H_5	OC_6H_5	−1.51	−1.69	AN	49
C_2H_5	C_6H_4-*p*-*n*-C_8H_{17}	−1.52	−1.73	DMF	50 [b]
C_6H_5	SC_6H_5	−1.37	−1.58	DMF	41
C_6H_5	SC_6H_5	−1.47	−1.68	DMF	45
C_6H_5	SC_6H_5	−1.35	−1.55	DMSO	40,47
C_6H_5	SC_6H_5	−1.45	−1.66	DMA	51
C_6H_5	SC_6H_5	−1.38	−1.56	AN	42
CH_2CH_2OH	SCH_2CH_2OH	−1.60	−1.80	DMSO	40
CH_2CH_2OH	SCH_2CH_2OH	−1.63	−1.82	DMF	45
CH_2CH_2OH	Cl	−1.22	−1.42	DMSO	40
C_6H_4-*p*-Cl	SC_6H_4-*p*-Cl	−1.22	−1.40	DMSO	40
C_6H_4-*p*-Cl	SC_6H_4-*p*-Cl	−1.30	−1.50	DMF	45
C_6H_4-*p*-CH_3	SC_6H_4-*p*-CH_3	−1.41	−1.61	DMSO	40
C_6H_4-*p*-CH_3	SC_6H_4-*p*-CH_3	−1.51	−1.69	DMF	45
C_6H_4-*p*-OCH_3	SC_6H_4-*p*-OCH_3	−1.53	−1.74	DMF	45
$CH_2C_6H_5$	$SCH_2C_6H_5$	−1.64	−1.86	DMF	45

[a] In ref. 46 redox potentials are also reported for the complete series $[Fe_6Mo_2S_8(\mu\text{-}SC_2H_5)_3\{Cl_{6-n}(SC_2H_5)_n\}]^{3-}$.

[b] In aqueous micellar solution (pH 7.0) a single two-electron (3−/5−) step is displayed at about −0.6 V (vs. SCE).

acterized by X-ray crystallography, permitting the evaluation of the stereochemical effect accompanying the overall redox change:

$$[Fe_6Mo_2S_8(SC_6H_5)_9]^{3-} \xrightarrow{+2e^-} [Fe_6Mo_2S_8(SC_6H_5)_9]^{5-}$$

A comparison of the structural parameters of the 3− /5− couple is reported in Table 7 [45].

The penta-anion maintains the starting double-cubane structure. The addition of an electron to each $MoFe_3S_4$ subunit simply causes core expansion, without any particular stereochemical distortion. The significant elongation of the $Fe–S(C_6H_5)_{(terminal)}$ has been interpreted in terms of the Fe–S character of the LUMO of the trianions; this datum is also supported by the sensitivity of the redox potentials (Table 6) to the different substituents [45].

TABLE 7

Comparison between selected structural parameters of $[Fe_6Mo_2S_8(SC_6H_5)_9]^{3-,5-}$ clusters [37,45]

Unit	Mean distance (Å)	
	$[Fe_6Mo_2S_8(SC_6H_5)_9]^{3-}$	$[Fe_6Mo_2S_8(SC_6H_5)_9]^{5-}$
Bridging unit		
Mo · · · Mo	3.68	3.81
Mo–S	2.58	2.62
$MoFe_3S_4(SC_6H_5)_3$ cubane subunit		
Mo–S	2.34	2.37
Fe–S	2.25	2.28
Fe–SC_6H_5	2.25	2.30
Mo · · · Fe	2.71	2.76

The ability of $[Fe_6Mo_2S_8(SR)_9]^{3-}$ to undergo the step-by-step two-electron 3 − /4 − /5 − reduction has recently been used to perform catalytic reductions of biological interest (RN_3 to NH_3 and N_2H_4 [52], NO_3^- to NH_3, and NO_2^- to N_2O [53]). The inverse pathway (5 − /3 −) can perform the two-electron oxidation of thiols (2PhSH) to H_2 and $2PhS^-$ [51].

$Fe_6Mo_2S_8$ derivatives of type **2** in Scheme 3 are reported to have basically the same double-cubane structure as derivatives **1** [54,55]. A significant difference lies in a reduced Mo · · · Mo distance in the bridging fragment (about 3.2 Å compared with 3.7 Å).

From the electrochemical viewpoint, while $[Fe_6Mo_2S_8(SC_6H_5)_6(OCH_3)_3]^{3-}$ reversibly undergoes the usual 3 − /4 − and 4 − /5 − reduction steps [40], $[Fe_6Mo_2S_8(SC(CH_3)_3)_6(OCH_3)_3]^{3-}$ displays the two reversible one-electron reductions (3 − /4 − and 4 − /5 −) and the two reversible one-electron oxidations (3 − /2 − and 2 − /1 −) [45] (Table 8).

While it has proven impossible to characterize the oxidized species (2 − and/or 1 −), the relevant 4 − and 5 − species have been characterized spectroscopically [45].

TABLE 8

Standard electrode potentials (in volts) for the redox processes of $[Fe_6Mo_2S_8(\mu\text{-}OCH_3)_3(SR)_6]^{3-}$

R	$E^{o'}_{3-/4-}$	$E^{o'}_{4-/5-}$	$E^{o'}_{3-/2-}$	$E^{o'}_{2-/1-}$	Solvent	Ref.
C_6H_5	−1.42	−1.62	–	–	DMSO	40
C_6H_5	−1.50	−1.70	−0.40	–	DMF	45
$C(CH_3)_3$	−1.85	−2.05	−0.20	−0.42	DMF	45

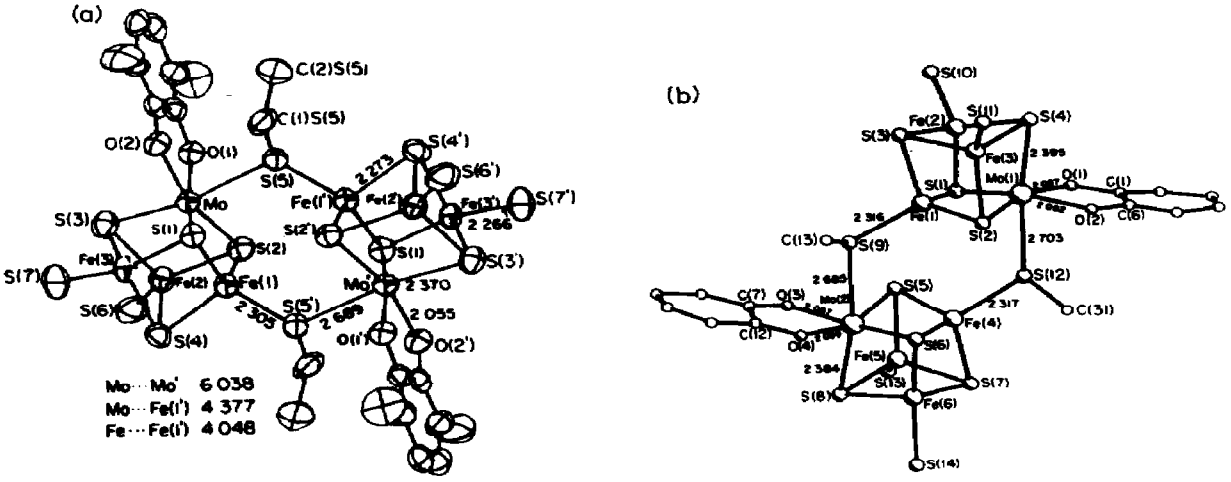

Fig. 16. Molecular structure (with selected mean distances) of: (a) $[Fe_6Mo_2S_8(SC_2H_5)_6\text{-}(3,6(n\text{-}C_3H_7)_2C_6H_4O_2)_2]^{4-}$ (from ref. 26); (b) $[Fe_6Mo_2S_8(SC_6H_4\text{-}p\text{-}Cl)_6(C_6H_4O_2)_2]^{4-}$ (from ref. 24).

Finally, the crystal structure of the double-cubane doubly bridged $Fe_6Mo_2S_8$ (3 in Scheme 4) is shown in Fig. 16 [24,26].

The cluster consists of two cubane-like $MoFe_3S_4$ subunits joined by two Mo(μ-SR)Fe bridges. The six bridging atoms are nearly coplanar. The elongated Mo–$S_{(bridging)}$ distance (about 2.7 Å) is assumed to be responsible for the facile cleavage leading to single-cubane iron–molybdenum clusters. Since this cleavage occurs in polar solvents, the electrochemistry of **3** clusters is indeed that of single-cubane Fe_3MoS_4 clusters (**1** in Scheme 2) discussed in Section B (ii) (h).

(m) $Fe_6Mo_2S_9$ core

Triply bridged double-cubane clusters having an $Fe_6Mo_2S_9$ core possess the following structure:

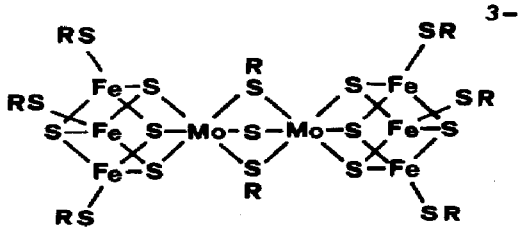

Scheme 5

The crystal structure of $[Fe_6Mo_2S_9(SC_2H_5)_8]^{3-}$ is shown in Fig. 17 [39,56].

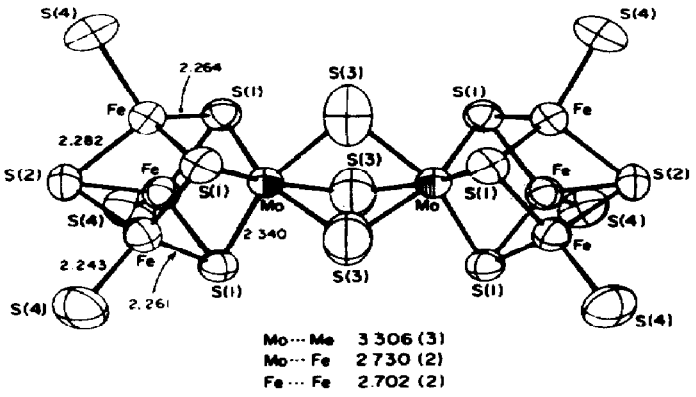

Fig. 17. Perspective view (with mean distances) of $[Fe_6Mo_2S_8(\mu\text{-}S)(\mu\text{-}SC_2H_5)_2(SC_2H_5)_6]^{3-}$ (from ref. 39).

The only significant difference with respect to the closely related $[Fe_6Mo_2S_8(SR)_9]^{3-}$ species (see Section B (ii) (l)) resides in the intercubane Mo · · · Mo distance, which in the bridging unit $Mo(\mu\text{-}SR)_3Mo$ is about 3.7 Å, while in the bridging unit $Mo(\mu\text{-}S)(\mu\text{-}SR)_2Mo$ is decidedly shorter (3.3 Å in the $[N(C_2H_5)_4]^+$ salt, 3.2 Å in the $[(C_2H_5)_3NCH_2(C_6H_5)]^+$ salt).

In accordance with the assumption that the addition of electrons to the double-cubane clusters is centered on the $MoFe_3S_4$ units, the following electron-transfer sequence occurs in acetonitrile at nearly the same potential as for the corresponding $Fe_6Mo_2S_8$ derivatives [42,44]:

$$[Fe_6Mo_2S_9(SC_2H_5)_8]^{3-} \overset{E^{\circ\prime} = -1.67\ V}{\underset{-e^-}{\overset{+e^+}{\rightleftarrows}}} [Fe_6Mo_2S_9(SC_2H_5)_8]^{4-} \overset{E^{\circ\prime} = -1.87\ V}{\underset{-e^-}{\overset{+e^-}{\rightleftarrows}}} [Fe_6Mo_2S_9(SC_2H_5)_8]^{5-}$$

(n) $Fe_6Mo_2S_{12}$ core

The most recently prepared member of the class of double-cubane iron–molybdenum clusters is $[Fe_6Mo_2S_{12}(SC_6H_4\text{-}p\text{-}X)_6]^{4-}$ (X = Cl, Br). It is constructed of two cubane units linked through two disulfide bridges (Fig. 18) [57]. The Mo · · · Mo distance in the bridging $Mo(S_2)_2Mo$ unit is 3.97 Å.

In acetonitrile, $[Fe_6Mo_2S_{12}(SC_6H_4\text{-}p\text{-}Cl)_6]^{4-}$ undergoes a one-electron oxidation ($E^{\circ\prime} = -0.52$ V) and two successive one-electron reductions ($E^{\circ\prime} = -1.52$ V and $E^{\circ\prime} = -1.72$ V respectively) [57]. As can be judged from the cathodic $\Delta E^{\circ\prime}$ value (0.2 V), the increased Mo · · · Mo distance,

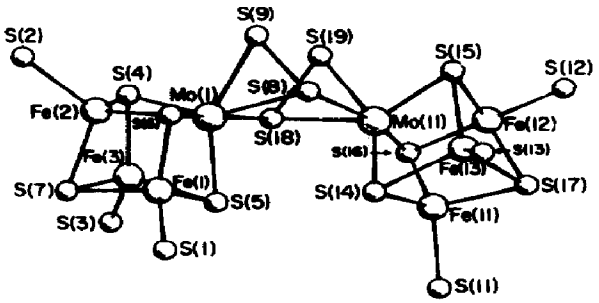

Fig. 18. Crystal structure of $[Fe_6Mo_2S_8(S_2)_2(SC_6H_4\text{-}p\text{-}Br)_6]^{4-}$ (from ref. 57).

compared with the previous distances, is still not sufficient to prevent the interaction between the two cubane subunits.

(o) $Fe_7Mo_2S_8$ core

As represented in Scheme 6, clusters containing an $Fe_7Mo_2S_8$ core have a structure in which two $MoFe_3S_4$ units are linked by an $Fe(SR)_6$ bridge.

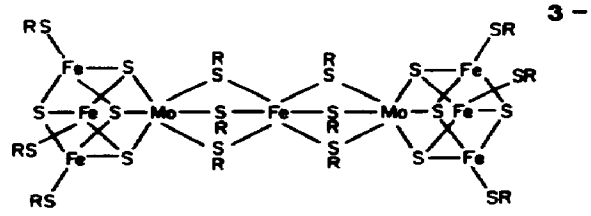

Scheme 6

Figure 19 refers to $[Fe_7Mo_2S_8(\mu_2\text{-}SC_2H_5)_6(SC_6H_5)_6]^{3-}$; these types of cluster undergo three consecutive one-electron cathodic reduction steps [42,44,48]. The less cathodic process corresponds to the bridge-centered Fe(III)/Fe(II) step, whereas the other processes involve the addition of one electron to each of the two $MoFe_3S_4$ subclusters, according to the following sequence (Table 9) [42]:

$$[Fe_7Mo_2S_8(SR)_{12}]^{3-} \underset{-e^-}{\overset{+e^-}{\rightleftarrows}} [Fe_7Mo_2S_8(SR)_{12}]^{4-} \underset{-e^-}{\overset{+e^-}{\rightleftarrows}} [Fe_7Mo_2S_8(SR)_{12}]^{5-} \rightleftarrows$$

$$\underset{-e^-}{\overset{+e^-}{\rightleftarrows}} [Fe_7Mo_2S_8(SR)_{12}]^{6-}$$

Synthetic procedures leading to both $[Fe_7Mo_2S_8(SR)_{12}]^{3-}$ and $[Fe_7Mo_2S_8(SR)_{12}]^{4-}$ have been proposed [44,58]. Figure 20 shows the typical molecular structure of the trianion and tetra-anion [58]. In both anions, the two $MoFe_3S_4$ cubane cores maintain the same dimensions and essentially the same trigonal distortion from cubic symmetry.

The main consequence of the one-electron reduction of the bridging Fe(III) atom is the remarkable elongation (about 0.3 Å) of the Mo · · · Mo

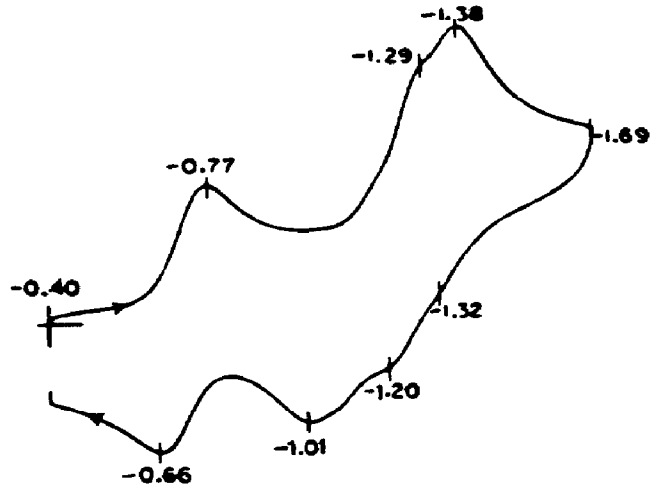

Fig. 19. Cyclic voltammogram of $[Fe_7Mo_2S_8(SC_2H_5)_6(SC_6H_5)_6]^{3-}$ recorded in acetonitrile (from ref. 48).

distance, probably owing to the presence of an Fe(II) ion larger than an Fe(III) ion.

Interestingly, in agreement with the long Mo · · · Mo distance in the bridging unit (6.6–6.9 Å), the difference in redox potentials between the cubane-centered $4-/5-$ and $5-/6-$ steps approaches the theoretical value of 36 mV foreseen for the successive addition of one electron into two non-interacting sites (see Section B (ii) (l)).

(iii) Iron–tungsten clusters

In many aspects, the chemistry of iron–tungsten–sulfur clusters parallels that of iron–molybdenum–sulfur clusters [1–4]. Therefore we shall frequently recall the preceding section.

(a) FeW_2S_8 core

While there is evidence that the dianion $[Fe(WS_4)_2]^{2-}$ possesses a linear

TABLE 9

Redox potentials (in volts) for the cathodic processes of $[Fe_7Mo_2S_8(\mu_2\text{-}SR)_6(X)_6]^{3-}$ in acetonitrile solvent [48]

R	X	$E^{\circ\prime}_{3-/4-}$	$E_{p_{4-/5-}}$	$E_{p_{5-/6-}}$
C_2H_5	SC_2H_5	−1.27	−1.95	−2.00
C_2H_5	SC_6H_5	−1.10	−1.67	−1.76
C_2H_5	Cl	−1.00	−1.52	−1.62

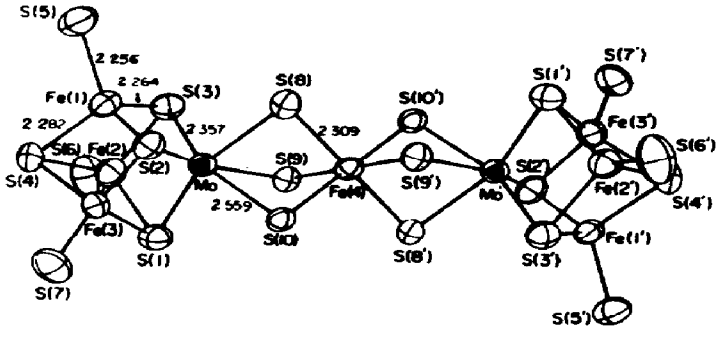

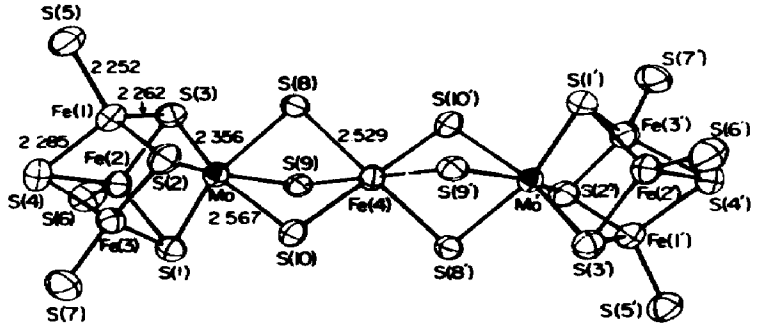

Fig. 20. Perspective view (with selected mean distances) of: (a) $[Fe_7Mo_2S_8(SC_2H_5)_{12}]^{3-}$; (b) $[Fe_7Mo_2S_8(SCH_2C_6H_5)_{12}]^{4-}$ (from ref. 58).

assembly with a central tetrahedrally coordinated FeS_4 unit [20], the only crystalline forms resolved are the two bis adducts (with DMF [59] and H_2O [60] respectively) shown in Fig. 21. The *trans* coordination of the two DMF or H_2O molecules imposes an octahedral geometry on the central Fe atom.

The species $[Fe(WS_4)_2]^{2-}$ undergoes, in DMF, a single quasi-reversible one-electron reduction process, according to the following sequence (Fig. 22) [61]:

$$[Fe(WS_4)_2]^{2-} \underset{-e^-}{\overset{+e^-}{\rightleftarrows}} [Fe(WS_4)_2]^{3-} \qquad E^{\circ\prime} = -0.72 \text{ V}$$

The same reduction process has been observed in dichloromethane at $E^{\circ\prime} = -0.64$ V [59]. This step must be assigned to the Fe(II)/Fe(I) charge transfer [19].

In agreement with the chemical reversibility of this one-electron reduction, the trianion $[Fe(WS_4)_2]^{3-}$ has been prepared and fully characterized

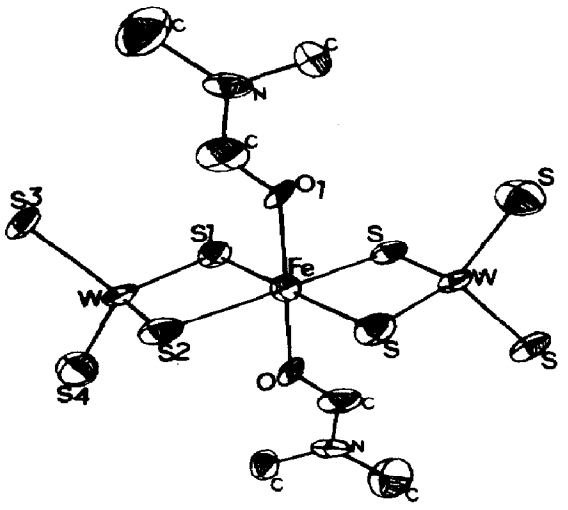

(a)

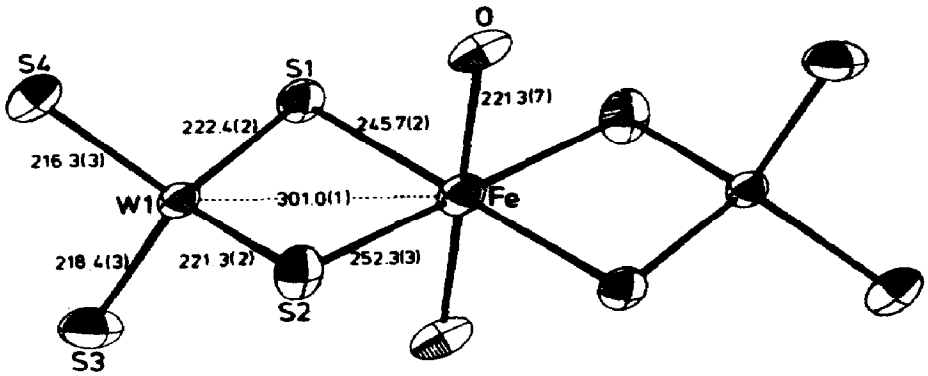

(b)

Fig. 21. Perspective view of: (a) $[Fe(WS_4)_2(DMF)_2]^{2-}$; (b) $[Fe(WS_4)_2(H_2O)_2]^{2-}$. Core mean distances: Fe–W (a) 3.04 Å, (b) 3.01 Å; Fe–S (a) 2.51 Å, (b) 2.49 Å; $W–S_{(bridging)}$ (a) 2.21 Å, (b) 2.21 Å; $W–S_{(terminal)}$ (a) 2.16 Å, (b) 2.17 Å (from refs. 59, 60, respectively).

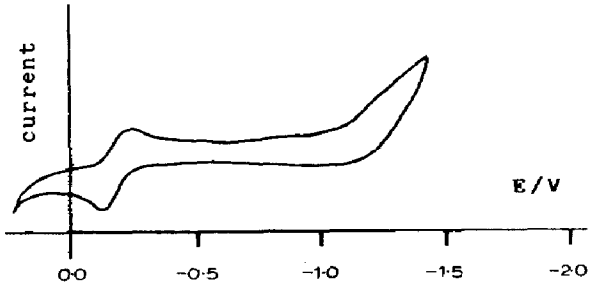

Fig. 22. Cyclic voltammogram recorded on $[Fe(WS_4)_2]^{2-}$ in dimethylformamide. Potential values vs. an Ag/AgCl/LiCl(sat), EtOH electrode (from ref. 61).

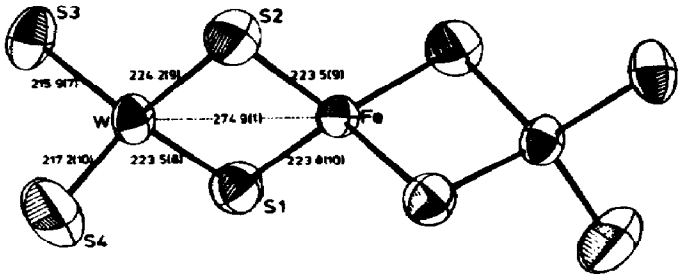

Fig. 23. Perspective view of the trianion $[Fe(WS_4)_2]^{3-}$. Distances in pm. W–$\widehat{Fe}$–W 171.2° (from ref. 62).

(Fig. 23) [62]. In this case, the central FeS_4 unit is really tetrahedrally coordinated. Because of the constraints present in the dinegative diadduct, straightforward evaluation of the stereochemical changes accompanying the $2-/3-$ charge transfer is prevented.

Deeper insight into the redox properties of $[Fe(WS_4)_2]^{3-}$ in acetonitrile [63] has, however, shown that there are four potentially stable members of this family, according to the following sequence:

$$[Fe(WS_4)_2]^{-} \underset{-e^-}{\overset{+e^-}{\rightleftarrows}} [Fe(WS_4)_2]^{2-} \underset{-e^-}{\overset{+e^-}{\rightleftarrows}} [Fe(WS_4)_2]^{3-} \underset{-e^-}{\overset{+e^-}{\rightleftarrows}} [Fe(WS_4)_2]^{4-}$$

$$E^{\circ\prime} = -0.21\ \text{V} \qquad E^{\circ\prime} = -0.65\ \text{V} \qquad E^{\circ\prime} = -2.45\ \text{V}$$

(b) Fe_2WS_4 core

The dianion $[Cl_2FeS_2WS_2FeCl_2]^{2-}$ is isostructural with its molybdenum analogue (Fig. 5) [22]. The intermetallic distances are generally slightly longer in the tungsten derivative than in the molybdenum derivative.

In dichloromethane the tungsten dianion undergoes a one-electron reduction ($2-/3-$) ($E_p = -1.33$ V) leading to the trianion, which decomposes to $[(WS_4)Fe_2Cl_3]^{2-}$ at a rate much faster than that in the case of the molybdenum derivative (see Section B (ii) (d)) [22].

The difference in redox potentials of about 0.3 V between the molybdenum and tungsten derivatives supports the view that the empty *d* orbitals of M(VI) (M = Mo, W) constitute the LUMO of these complexes.

(c) Fe_3WS_4 core

The single-cubane Fe_3WS_4 clusters characterized until now are represented in Scheme 7.

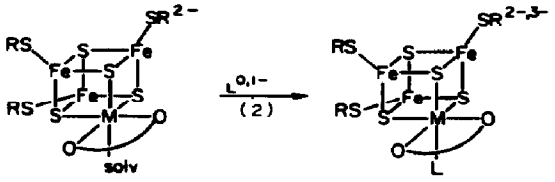

L = RS^-, CN^-

M = W

$\overset{\frown}{O\ O}$ = 3,6-$(C_3H_5)_2C_6H_2O_2$

Scheme 7

These catecholate clusters, both in the solvated and ligated forms, contain the $[WFe_3S_4]^{3+}$ core and are isostructural with the corresponding molybdenum derivatives (see Section B (ii) (h)); furthermore, they undergo both a reversible one-electron oxidation and a reversible one-electron reduction (Table 10). Comparison with the molybdenum analogues reveals that for the tungsten derivatives the core oxidation level of 2+ is less accessible (by about 0.2 V), whereas the core oxidation level of 4+ is more easily accessible (by about 0.1 V).

Spectroscopic characterization of the one-electron reduced solvated and ligated clusters has been reported [27].

(d) $Fe_6W_2S_6$ core

The tungsten analogue of the $Fe_6Mo_2S_6$ core, shown in Section B (ii) (k) has been prepared in the form of the trianion $[Fe_6S_6(OC_6H_4$-*p*-$CH_3)_6\{W(CO)_3\}_2]^{3-}$ (Fig. 24) [35].

TABLE 10

Standard electrode potentials (in volts) for the redox changes of the $[Fe_3WS_4]^{3+}$ core in the single cubanes illustrated in Scheme 7

R	L	$E^{o\prime}_{3+/2+}$	$E^{o\prime}_{3+/4+}$	Solvent	Ref.
Solvated clusters					
C_6H_4-*p*-Cl	–	−1.60	−0.55	AN	27
C_6H_4-*p*-Cl	–	−1.75	−0.73	DMF	27
C_6H_4-*p*-Cl	–	−1.72	−0.57 [a]	DMSO	27
C_2H_5	–	−1.98	−0.90	DMSO	27
C_6H_5	–	−1.78	–	DMSO	26
Ligated clusters					
C_6H_4-*p*-Cl	SC_6H_4-*p*-Cl	−1.65	−0.81 [a]	AN	27
C_6H_4-*p*-Cl	CN	−1.83	−0.70	AN	27
C_2H_5	CN	−2.15	−1.01	AN	27

[a] Peak potential values for irreversible processes.

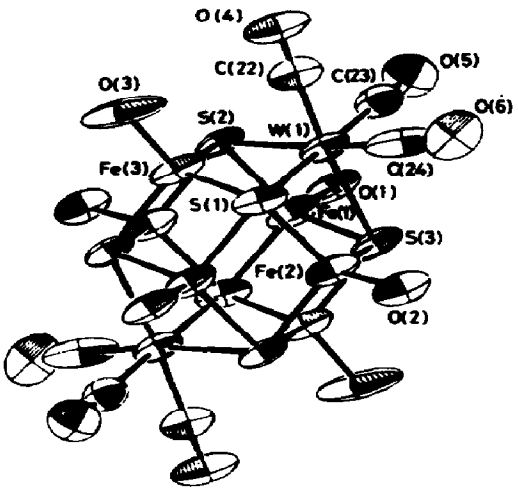

Fig. 24. Perspective view of $[Fe_6S_6(OC_6H_4\text{-}p\text{-}CH_3)_6\{W(CO)_3\}_2]^{3-}$ (from ref. 35).

The $[Fe_6W_2(\mu\text{-}S)_6]^{3+}$ core is described as an Fe_6W_2 cube having the two W atoms at opposite corners on the body diagonal. Each WFe_3 face of this cube is bonded to a quadruply bridging S atom. The elongation of the cube along the body diagonal causes the core to assume a hexagonal prismatic D_{3d} symmetry [35].

In dichloromethane, this $Fe_6W_2S_6$ derivative undergoes two reversible one-electron cathodic processes [35] according to the following sequence:

$$[Fe_6W_2S_6]^{3+} \underset{-e^-}{\overset{+e^-}{\rightleftarrows}} [Fe_6W_2S_6]^{2+} \quad (E^{\circ\prime} = -0.87\ \text{V}) \qquad [Fe_6W_2S_6]^{2+} \underset{-e^-}{\overset{+e^-}{\rightleftarrows}} [Fe_6W_2S_6]^{+} \quad (E^{\circ\prime} = -1.36\ \text{V})$$

This redox behavior is quite similar to that displayed by the molybdenum analogue [33].

Characterizations of the probably stable tetra-anion and penta-anion have not yet appeared.

(e) $Fe_6W_2S_8$ core

As seen in Section (B) (ii) (l) the $M_2Fe_6S_8$ core (M = W, Mo) is present in both triply bridged double-cubane clusters, **1** ($[W_2Fe_6S_8(\mu\text{-}L')_3(L)_6]^{3-}$) in Scheme 8, and doubly bridged double-cubane clusters **2** ($[W_2Fe_6S_8(\mu\text{-}SR)_2(SR)_4(\text{catecholate})_2]^{4-}$).

Considering the triply bridged derivatives, contrary to the $Mo_2Fe_6S_8$ derivatives which reversibly undergo the $3-/4-$ and $4-/5-$ reduction steps, the $W_2Fe_6S_8$ derivatives undergo these steps with a degree of reversibility which is highly dependent upon the solvent [40,46]. Unfortunately no

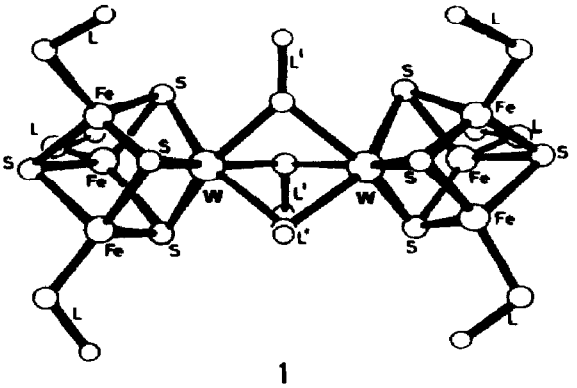

1

L= L'= SC_2H_5

L= SC_6H_5, L'= OCH_3

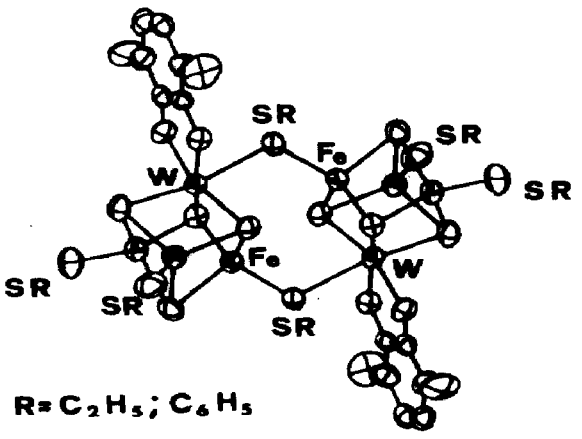

R= C_2H_5; C_6H_5

2

Scheme 8

redox potentials are available in acetonitrile, in which these charge transfers occur reversibly [40,64]. This difference in electron-transfer ability between the isostructural Fe–Mo–S and Fe–W–S clusters could be responsible for the failure of the latter synthetic clusters to mimic functional nitrogenases [43,46,64].

In polar solvents the doubly bridged double-cubane derivatives undergo bridge cleavage leading to single-cubane Fe_3WS_4 species [26].

Hence there is no electrochemical behavior specific for these clusters.

(f) $Fe_6W_2S_9$ core

The $Fe_6W_2S_9$ core is present in the triply bridged $[(\mu\text{-S})(\mu\text{-SR})_2]$ double cubanes represented in Scheme 9. Indeed the only electrochemically char-

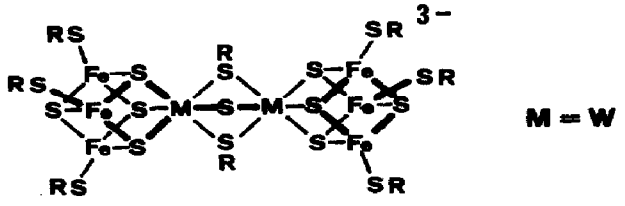

M = W

Scheme 9

acterized member of this family is $[Fe_6W_2S_8(\mu\text{-S})(\mu\text{-SC}_2H_5)_2(SC_2H_5)_6]^{3-}$,

which in acetonitrile reversibly undergoes the usual closely-spaced 3 − /4 − and 4 − /5 − reduction steps according to the following sequence:

$$[Fe_6W_2S_9(SC_2H_5)_8]^{3-} \overset{E^{\circ\prime} = -1.79\ V}{\underset{-e^-}{\overset{+e^-}{\rightleftarrows}}} [Fe_6W_2S_9(SC_2H_5)_8]^{4-} \overset{E^{\circ\prime} = -1.98\ V}{\underset{-e^-}{\overset{+e^-}{\rightleftarrows}}} [Fe_6W_2S_9(SC_2H_5)_8]^{5-}$$

(g) $Fe_7W_2S_8$ core

Clusters containing the $Fe_7W_2S_8$ core are represented in Scheme 10. As in

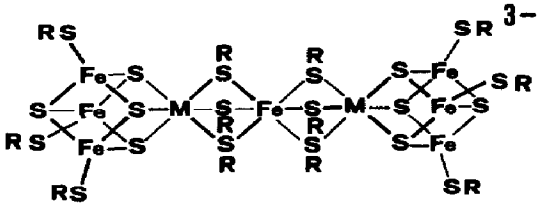

Scheme 10

the case of their molybdenum analogues, these species undergo first a one-electron reduction process centered on the bridging Fe(III) unit, followed by two near-merging successive one-electron reduction steps, each of one is centered on the WFe_3S_4 subclusters [42,44]. In acetonitrile the following sequence has been verified:

$$[Fe_7W_2S_8(SC_2H_5)_{12}]^{3-} \overset{E^{\circ\prime} = -1.14\ V}{\underset{-e^-}{\overset{+e^-}{\rightleftarrows}}} [Fe_7W_2S_8(SC_2H_5)_{12}]^{4-} \overset{E_p = -2.08\ V}{\underset{-e^-}{\overset{+e^-}{\rightleftarrows}}} [Fe_7W_2S_8(SC_2H_5)_{12}]^{5-} \overset{E_p = -2.18\ V}{\underset{-e^-}{\overset{+e^-}{\rightleftarrows}}} [Fe_7W_2S_8(SC_2H_5)_{12}]^{6-}$$

The one-electron reduced species $[Fe_7W_2S_8(SC_2H_5)_{12}]^{4-}$ has been isolated and spectroscopically characterized [42,44].

(iv) Iron–vanadium clusters

The characterization of iron–vanadium clusters is fairly recent. Many derivatives have not been studied electrochemically, namely VFe_2S_4 [65,66], V_2FeS_3 [67,68], V_2FeS_4 [67–69] and $V_2Fe_2S_4$ [69] cores.

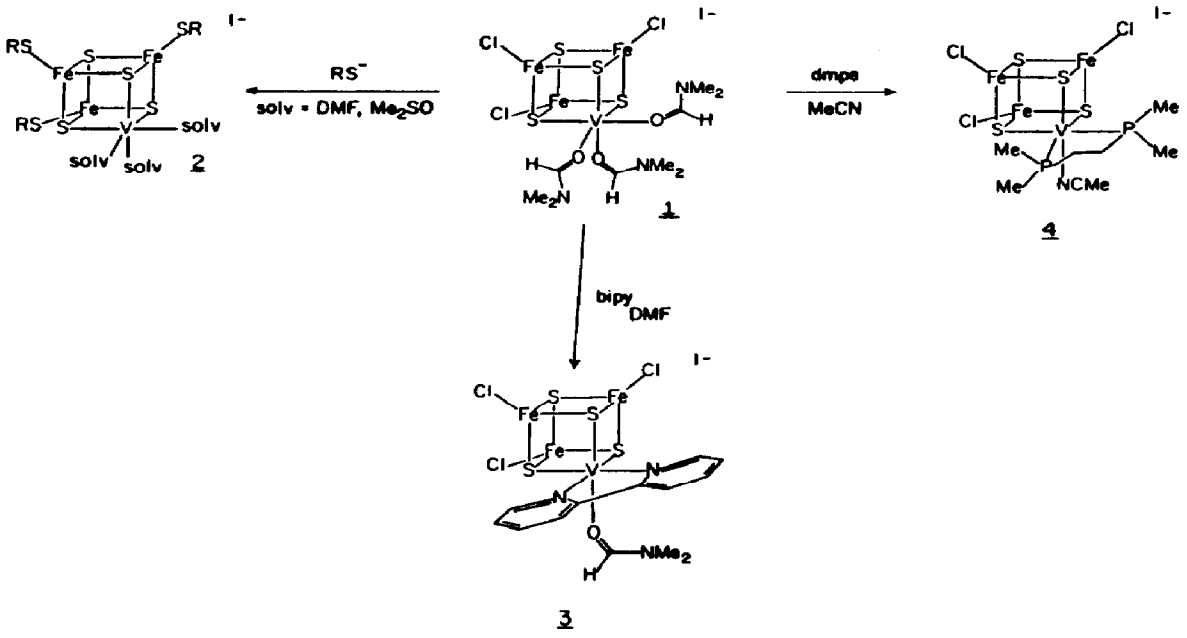

Scheme 11

(a) Fe_3VS_4 core

A series of compounds containing the Fe_3VS_4 assembly have recently been prepared [70–72]. These single-cubane derivatives, illustrated in Scheme 11, contain an $[Fe_3VS_4]^{2+}$ core, isoelectronic with $[Fe_3MoS_4]^{3+}$ and $[Fe_3WS_4]^{3+}$, discussed in Sections B (ii) (h) and B (iii) (c) respectively.

In comparison with the corresponding molybdenum or tungsten clusters, the ability of the vanadium site to be bonded to three monodentate ligands is very evident, whereas the molybdenum site always binds one labile ligand and one bidentate (catecholate or dimethylphosphinoethane) ligand.

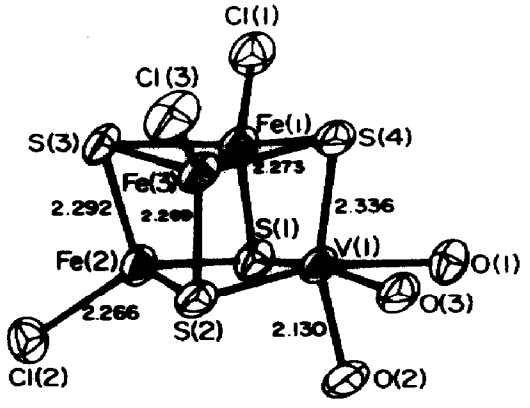

Fig. 25. X-ray structure of $[Fe_3VS_4Cl_3(DMF)_3]^-$ (from ref. 73).

TABLE 11

Redox potentials (in volts) for the charge transfers exhibited by Fe_3VS_4 species [72]

Cluster	$E^{\circ\prime}_{1-/0}$	$E_{p1-/2-}$	Solvent
$[Fe_3VS_4Cl_3(DMF)_3]^-$	−0.47	−1.83	DMF
$[Fe_3VS_4Cl_3(AN)_3]^-$	−0.26	−1.53	AN
$[Fe_3VS_4Cl_3(bpy)(DMF)]^-$ [a]	−0.07 [c]	−1.65	DMF
$[Fe_3VS_4Cl_3(dmpe)(AN)]^-$ [b]	−0.35	−1.66	AN
$[Fe_3VS_4(SC_6H_4\text{-}p\text{-}CH_3)(DMF)_3]^-$	−0.76	−1.80	DMF

[a] bpy = 2,2′-dipyridyl.

[b] dmpe = 1,2-bis(dimethylphosphino)ethane.

[c] Peak potential value for irreversible processes.

The crystal structure of $[Fe_3VS_4Cl_3(DMF)_3]^-$ is reported in Fig. 25 as a typical example of the $[Fe_3VS_4]^{2+}$ core. The cubane Fe_3VS_4 moiety (9.62 Å^3) of idealized C_{3v} symmetry consists of two interpenetrating irregular VFe_3 and S_4 tetrahedra. The FeS_3Cl units are trigonally distorted tetrahedra; the vanadium site exhibits distorted octahedral coordination [73].

When two of the three molecules of DMF coordinated to the vanadium site are substituted by one chelating molecule of 2,2′-bipyridyl or 1,2-bis(dimethylphosphino)ethane, the symmetry is degraded to C_s, but the core dimensions remain substantially invariant [73].

Although a detailed study of the electronic properties of the $[Fe_3VS_4]^{2+}$ and $[Fe_3MS_4]^{3+}$ (M = Mo, W) units shows very close resemblance between them [74], their redox properties are significantly different. In fact, while $[Fe_3MS_4]^{3+}$ (M = Mo, W) derivatives generally reversibly undergo both a one-electron oxidation and a one-electron reduction, the $[Fe_3VS_4]^{2+}$ derivatives are usually inclined to a reversible one-electron oxidation and to reductions complicated by subsequent (probably declustering) reactions [72] (Table 11).

The tendency towards reversible oxidation but irreversible reduction has been interpreted, on the basis of the isomer shift study [74], in terms of the presence of Fe atoms in vanadium clusters slightly more reduced than those in molybdenum clusters.

The reversibility of the charge transfer $[Fe_3VS_4]^{2+/3+}$ would allow the isolation of the one-electron oxidation products; hence it will be possible to evaluate the stereochemical consequences of the removal of one electron from the Fe_3VS_4 cubane core.

(b) $Fe_6V_2S_8$ core

As shown in Scheme 12, the reaction between single-cubane Fe_3VS_4 species and ethane-1,2-dithiolate leads to a doubly bridged double-cubane

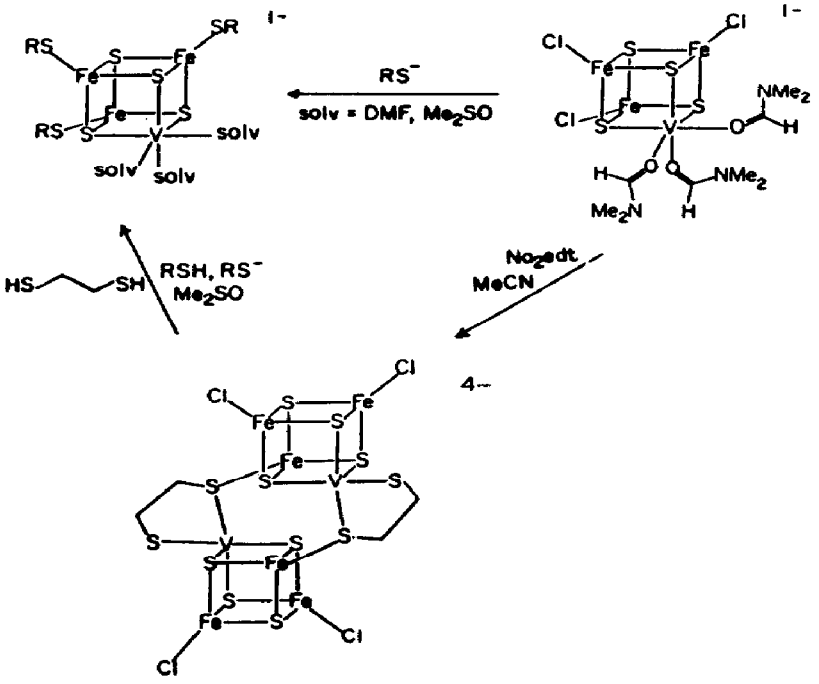

Scheme 12

derivative [72] which has many analogies with the previously discussed double cubanes $[Fe_6M_2S_8(SR)_6(catecholate)_2]^{4-}$ (M = Mo, W).

In this centrosymmetric molecule (Fig. 26) the two Fe_3VS_4 cubane subclusters, geometrically similar to those previously described, are connected through two Fe–(μ-S)–V bridges.

Interestingly, this double-cubane species is stable in coordinating solvents, contrary to the catecholate double-cubane Mo or W species, which are cleaved to solvated single cubanes. This fact is attributed to the $V-S_{(bridging)}$ distance ($\sim$ 2.5 Å) being significantly shorter (0.2 Å) than the $Mo-S_{(bridging)}$. This allows one to define its redox behavior in non-aqueous solvents. Unfortunately the electrochemistry is not exciting, in that $[Fe_6S_8V_2Cl_4(edt)_2]^{4-}$ undergoes in DMF two irreversible anodic processes at -0.73 V and -0.58 V respectively [72]. It is likely that the two steps correspond to the removal of one electron from each cubane unit.

(v) Cobalt–molybdenum clusters

A series of cobalt–molybdenum complexes of general formula $[Co(MoO_{4-n}S_n)_2]^{x-}$ ($x = 2, 3$; $n = 2, 3, 4$) has been characterized.

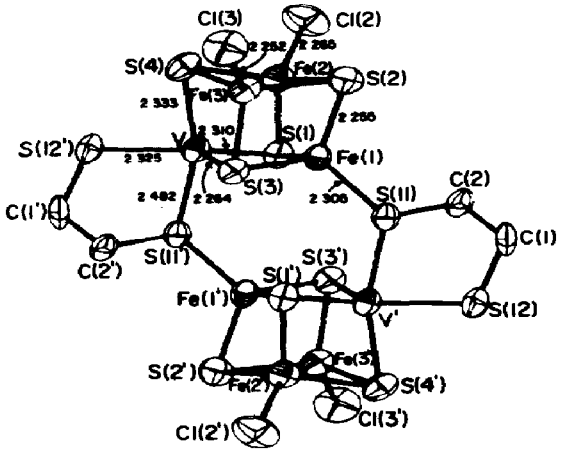

Fig. 26. Molecular structure of $[Fe_6V_2S_8Cl_4(edt)_2]^{4-}$ (edt = ethane-1,2-dithiolate) (from ref. 72).

(a) $CoMo_2S_8$ core

The dianion $[Co(MoS_4)_2]^{2-}$ cannot be isolated in a pure form, but it can be readily obtained in solution in organic solvents [75]. In dimethylformamide, it undergoes a reversible one-electron reduction step ($E^{\circ\prime} = -0.82$ V) leading to the stable trianion $[Co(MoS_4)_2]^{3-}$ [75]. The trianion has been structurally characterized (Fig. 27) [60,75]. Unfortunately, at the present stage, we cannot evaluate the stereochemical effect of the redox change $[Co(MoS_4)_2]^{2-/3-}$ (except by extrapolation with the corresponding compound in the tetrathiotungstate series (see Section B (vi) (a)).

On the basis of a molecular orbital study, it is, however, expected that the dianion possesses (i) longer Co–Mo distances, (ii) shorter Co–S distances, (iii) shorter $Mo–S_{(terminal)}$ distances and (iv) invariant $Mo–S_{(bridging)}$ distances [76].

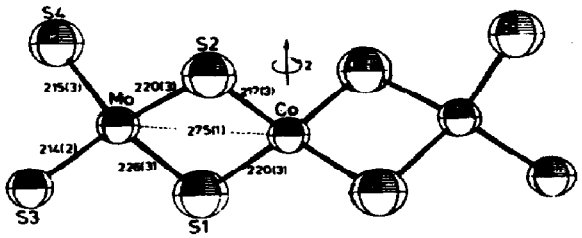

Fig. 27. Perspective view of $[Co(MoS_4)_2]^{3-}$. Mean distances in pm. Mo–$\widehat{Co}$–Mo 169.6° (from ref. 60).

(b) $CoMo_2S_6$ core

The thiooxomolybdate dianion $[Co(MoOS_3)_2]^{2-}$ cannot be obtained as the pure salt [75].

The structure assigned to it is of the type illustrated in Scheme 13 [75].

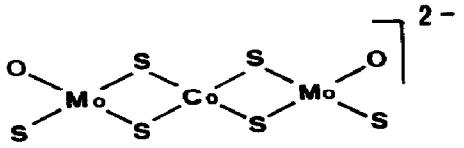

Scheme 13

Dimethylformamide solutions of this dianion show that it can be reversibly reduced to the likely stable trianion $[Co(MoOS_3)_2]^{3-}$ at $E^{\circ\prime} = -0.90$ V [75].

(c) $CoMo_2S_4$ core

On the basis of spectroscopic properties, the structural unit shown in Scheme 14 has been assigned to the thiooxomolybdate anion $[Co(MoO_2S_2)]^{2-}$, with the central cobalt atom having tetrahedral coordination [75,77,78].

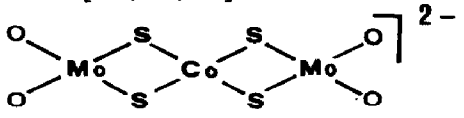

Scheme 14

In dimethylformamide the following reversible one-electron redox change occurs [61,75]:

$$[Co(MoO_2S_2)]^{2-} \underset{-e^-}{\overset{+e^-}{\rightleftarrows}} [Co(MoO_2S_2)]^{3-} \qquad E^{\circ\prime} = -1.23 \text{ V}$$

Spectral characterization of the trianion has been reported [75].

The easy access to the trianions, as the sulfur content of thiometallate dianions increases, has been attributed to the greater extent of dispersion of the low-lying *d* orbitals of the sulfur atom, which, favoring the electron delocalization within the molecular framework, depletes the electron density on the metals [75].

A quite different $CoMoS_4$ assembly has appeared very recently and will be discussed briefly in the Appendix.

(vi) Cobalt–tungsten clusters

The cobalt–tungsten complexes examined here belong to the family $[Co(WO_{4-n}S_n)_2]^{2-}$, in which n is equal to 4, 3 and 2 respectively.

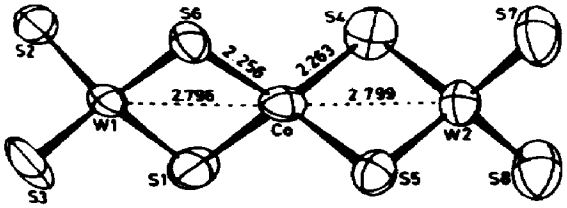

Fig. 28. Perspective view (together with some selected interatomic distances) of $[Co(WS_4)_2]^{2-}$ (from ref. 80).

(a) CoW_2S_8 core

The crystal structure of the dianion $[Co(WS_4)_2]^{2-}$ is shown in Fig. 28 [79,80]. This "linear" trimetallic assembly consists of the usual central metal atom (Co) nearly tetrahedrally coordinated by two bidentate chelating tetrathiotungstate anions. The species $[Co(WS_4)_2]^{2-}$ undergoes two probably reversible, one-electron reduction steps in dimethylformamide (Fig. 29). It is evident therefore that the $S_2WS_2CoS_2WS_2$ core is able to exist in three different oxidation levels [80]:

$$[Co(WS_4)_2]^{2-} \underset{-e^-}{\overset{+e^-}{\rightleftarrows}} [Co(WS_4)_2]^{3-} \underset{-e^-}{\overset{+e^-}{\rightleftarrows}} [Co(WS_4)_2]^{4-}$$

$$E^{\circ\prime} = -1.00\ \text{V} \qquad E^{\circ\prime} = -2.6\ \text{V}$$

The trianion has been isolated (Fig. 30) [75,81,82].

The redox $2-/3-$ change is accompanied by a contraction of the $WS_2Co_2S_2W$ core together with elongation of the $W-S_{(terminal)}$ bonds. This is the only example we know which allows an evaluation of the structural consequence of redox changes in linear trimetallic assemblies.

(b) CoW_2S_6 core

The monooxotrithiotungstate dianion $[Co(WOS_3)_2]^{2-}$ has the same geometry as $[Co(WS_4)_2]^{2-}$, with the oxygen atom of each $[WOS_3]^{2-}$ fragment occupying one of the two terminal positions [75,83,84].

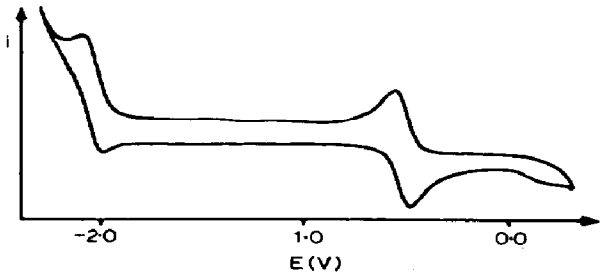

Fig. 29. Cyclic voltammogram recorded in a dimethylformamide solution of $[Co(WS_4)_2]^{2-}$. Potential values vs. Ag/AgCl/LiCl(sat), EtOH (from ref. 80).

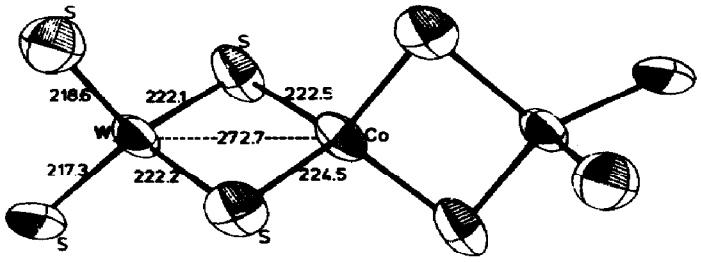

Fig. 30. Crystal structure of $[Co(WS_4)_2]^{3-}$. Mean distances in pm. W–$\widehat{Co}$–W 168.3° (from ref. 81).

In dimethylformamide the reversible one-electron reduction $[Co(WOS_3)_2]^{2-}/[Co(WOS_3)_2]^{3-}$ occurs at -1.07 V [60,75], i.e. at potentials only slightly more negative than those of the tetrathiotungstate analogue.

The trianion has been characterized spectroscopically [75].

(c) CoW_2S_4 core

Once again, an assembly similar to that represented in Scheme 14 has been proposed for the dioxodithiotungstate $[Co(WO_2S_2)_2]^{2-}$, with the four oxygen atoms occupying all the terminal positions [75,78,84].

In accordance with the fact that the gradual substitution of soft sulfur atoms with hard oxygen atoms makes the reduction processes more difficult, the $[Co(WO_2S_2)_2]^{2-}/[Co(WO_2S_2)_2]^{3-}$ reduction step occurs at $E^{\circ\prime} = -1.29$ V in dimethylformamide [75].

(vii) Cobalt–ruthenium clusters

(a) Co_2RuS core

The recently prepared $Co_2Ru(CO)_9(\mu_3\text{-}S)$ derivative [85] belongs to the family of triangular trimetallic clusters capped by one triply bridging sulfur atom (Fig. 31); it is the analogue of $Co_2FeS(CO)_9$ discussed in Section B (i) (a). As in the case of $Co_2FeS(CO)_9$, the most significant redox change for $Co_2RuS(CO)_9$ is the quasi-reversible charge transfer:

$$Co_2RuS(CO)_9 \underset{-e^-}{\overset{+e^-}{\rightleftarrows}} [Co_2RuS(CO)_9]^{\cdot}$$

which occurs at $E^{\circ\prime} = -1.20$ V in dichloroethane [14].

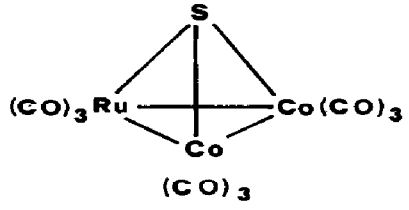

Fig. 31. Schematic representation of the structure of $Co_2RuS(CO)_9$.

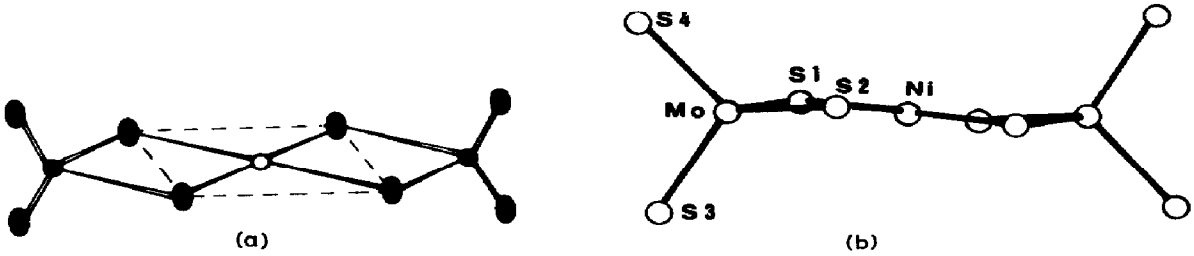

Fig. 32. Schematic representation (a) (from ref. 87) and perspective view (b) (from ref. 86) of the dianion $[Ni(MoS_4)_2]^{2-}$.

The sensitivity of the redox potential of the $0/1-$ step in the series $Co_2MS(CO)_9$ (M = Co, $E^{\circ\prime} = -1.10$ V; M = Fe, $E^{\circ\prime} = -1.05$ V; M = Ru, $E^{\circ\prime} = -1.20$ V) [14] confirms that the LUMO of these derivatives is essentially metal based.

At present, no data are available about the likely stable $[Co_2RuS(CO)_9]^{-}$.

(viii) Nickel–molybdenum clusters

As in the case of cobalt–molybdenum and cobalt–tungsten clusters, the nickel–molybdenum clusters presented here are included in the series $[Ni(MoO_{4-n}S_n)_2]^{2-}$, n varying from 4 to 2.

(a) $NiMo_2S_8$ core

Figure 32 shows the molecular structure of $[Ni(MoS_4)_2]^{2-}$ [86,87]. The dianion consists of a rigorously planar central NiS_4 group (Ni–S, 2.23 Å) coordinated by two molybdenum centers involved in a distorted tetrahedral geometry (Mo–$S_{(bridging)}$, 2.23 Å; Mo–$S_{(terminal)}$, 2.15 Å). The whole core MoS_2NiS_2Mo (Mo $\cdots$ Ni, 2.80 Å) is not planar since the planes NiS_1S_2 and MoS_1S_2 form an angle of 169.0° [86]. As indicated in Fig. 33, $[Ni(MoS_4)_2]^{2-}$ undergoes two consecutive reversible one-electron reduction processes in non-aqueous solvents, according to the following sequence (Table 12) [87,88]:

$$[Ni(MoS_4)_2]^{2-} \underset{-e^-}{\overset{+e^-}{\rightleftarrows}} [Ni(MoS_4)_2]^{3-} \underset{-e^-}{\overset{+e^-}{\rightleftarrows}} [Ni(MoS_4)_2]^{4-}$$

The fact that the first reduction processes occurs at the same potential as for $[Ni(WS_4)_2]^{2-}$ (Section B (ix) (a)) has suggested that the first electron is added to the central nickel moiety, i.e. the LUMO is essentially localized on the nickel atom [87]. More recent calculations, however, have led to the conclusion that the LUMO of the dianion is centered on low lying molybdenum *d* orbitals [89].

The electrogenerated trianion $[Ni(MoS_4)_2]^{3-}$ has been characterized by electron spin resonance (ESR) spectroscopy [89].

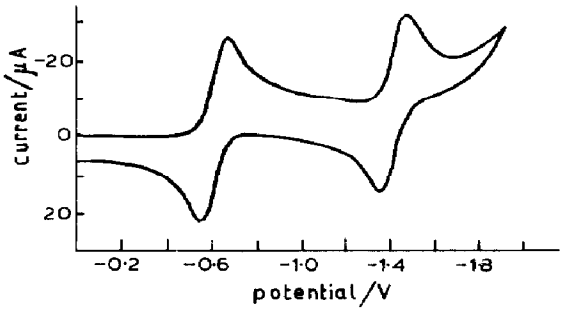

Fig. 33. Cyclic voltammetric behaviour of $[Ni(MoS_4)_2]^{2-}$ in dimethylformamide solvent. Potential values vs. SCE (from ref. 87).

(b) $NiMo_2S_6$ core

The dianion $[Ni(MoOS_3)_2]^{2-}$ is thought to have the same square-planar coordination as $[Ni(MoS_4)_2]^{2-}$, the only difference being the presence of a terminal oxygen atom in each of the two lateral $[MoOS_3]^{2-}$ fragments [77].

The one-electron reversible step $[Ni(MoOS_3)_2]^{2-/3-}$ takes place at $E°' = -1.13$ V in dimethylformamide [61].

(c) $NiMo_2S_4$ core

The dianion $[Ni(MoO_2S_2)_2]^{2-}$ probably possesses the same structure as represented in Scheme 14 for $[Co(MoO_2S_2)_2]^{2-}$, but with the central rigidly planar NiS_4 moiety [77,78].

The usual $[Ni(MoO_2S_2)_2]^{2-/3-}$ redox change occurs at $E°' = -1.17$ V in dimethylformamide [61], obeying the trend according to which the reduction step is more and more difficult in the order $[M(M'S_4)_2]^{2-} > [M(M'OS_3)_2]^{2-} > [M(M'O_2S_2)_2]^{2-}$.

(ix) Nickel–tungsten clusters

As with the trimetallic cobalt–molybdenum, cobalt–tungsten and nickel–molybdenum derivatives, the electrochemically active nickel–tungsten clusters belong to the $[Ni(WO_{4-n}S_n)_2]^{2-}$ family, n varying from 4 to 2.

TABLE 12

Standard electrode potentials (in volts) for the reduction processes of $[Ni(MoS_4)_2]^{2-}$

$E^{o'}_{2-/3-}$	$E^{o'}_{3-/4-}$	Solvent	Ref.
−0.92	−1.69	AN [a]	87
−0.65	–	DCM	89
−1.06	−1.85	DMF [a]	87

[a] $(C_2H_5)_4NClO_4$ supporting electrolyte.

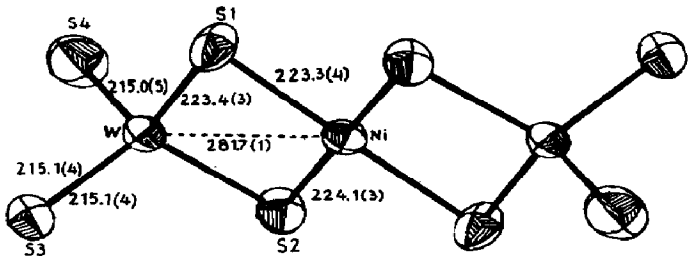

Fig. 34. Perspective view of $[Ni(WS_4)_2]^{2-}$. Distances in pm (from ref. 92).

(a) NiW_2S_8 core

The dianion $[Ni(WS_4)_2]^{2-}$ is isostructural with $[Ni(MoS_4)_2]^{2-}$ (Fig. 34) [90–92]. It undergoes two sequential reversible one-electron reduction steps [87,88], the potentials of which are reported in Table 13.

Comparison with the tetrathiomolybdate analogue shows that while the $2-/3-$ reduction step occurs at nearly the same potentials, the $3-/4-$ step is significantly more negative (about 0.2 V).

These results have been interpreted in terms of sequential occupation of an a_g molecular orbital (the nickel d_{xy} orbital), with pairing energies increasing with the mass of the lateral anions (MoS_4^{2-} or WS_4^{2-}) [87]. However, as previously noted it has more recently been calculated that the LUMO of these complexes is an a_g molecular orbital composed of the molybdenum $d_{x^2-y^2}$ and d_{z^2} orbitals [89].

The trianion $[Ni(WS_4)_2]^{3-}$ has been characterized by ESR measurements [89].

(b) NiW_2S_6 core

The structure proposed for the monooxotrithiotungstate anion $[Ni(WOS_3)_2]^{2-}$ is shown in Fig. 35 [83]. This dianion undergoes the $2-/3-$ step at $E^{\circ\prime} = -1.13$ V in dimethylformamide [61]. As usual, the presence of an oxygen atom substituting a sulfur atom makes the reduction slightly more difficult.

TABLE 13

Redox potentials (in volts) for the reduction processes of $[Ni(WS_4)_2]^{2-}$

$E^{\circ\prime}_{2-/3-}$	$E^{\circ\prime}_{3-/4-}$	Solvent	Ref.
−0.94	−1.87	AN	87
−1.06	−2.02	DMF	87
−0.66	–	DCM	89

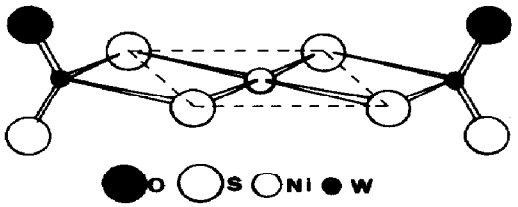

Fig. 35. Proposed structure of $[Ni(WOS_3)_2]^{2-}$ (*cis*-form) (from ref. 83).

(c) NiW_2S_4 core

The structure assigned to the dioxodithiotungstate anion $[Ni(WO_2S_2)_2]^{2-}$ is represented in Fig. 36 [84]. The $2-/3-$ reduction step occurs at $E^{\circ\prime} = -1.23$ V in dimethylformamide [61].

Table 14 summarizes the redox potentials for the first cathodic process in the series $[M(M'O_{4-n}S_n)_2]^{2-}$. Within the different families, the differences in redox potentials are markedly small, indicating that solvation effects practically make them indistinguishable if the LUMO of these complexes is centered on M or M'. Probably only in the case $[Fe(WS_4)_2]^{2-}$ is the electron added to the central FeS_4 unit [19].

(x) Copper–tungsten clusters

(a) Cu_2WS_4 core

Figure 37 shows the molecular structure of the dianion $[Cu_2Cl_2WS_4]^{2-}$ [93]. In this nearly linear Cu–W–Cu assembly, the central W(VI) atom is tetrahedrally coordinated in a trigonal planar geometry.

In dimethylformamide, $[Cu_2Cl_2WS_4]^{2-}$ undergoes an irreversible (probably declustering) anodic process ($E_p = 0.0$ V) attributed to the oxidation of the copper(I) centres [93].

(b) Cu_3WS_4 core

The structure of the dianion $[Cu_3Cl_3WS_4]^{2-}$ is shown in Fig. 38 [94,95]. It consists of a central WS_4^{2-} tetrahedron linked to three CuCl fragments. Each copper center has a trigonal planar coordination geometry.

In dimethylformamide, $[Cu_3Cl_3WS_4]^{2-}$ undergoes an oxidation process

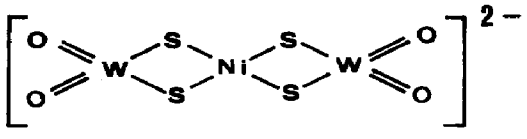

Fig. 36. Proposed structure for $[Ni(WO_2S_2)_2]^{2-}$. WO_2 planes are likely to be perpendicular to WS_2 planes.

TABLE 14

Redox potentials (in volts) for the 2−/3− step of $[M(M'O_{4-n}S_n)_2]^{2-}$ (M = Fe, Co, Ni; M′ = Mo, W) in dimethylformamide

Compound	$E^{\circ\prime}_{2-/3-}$	Compound	$E^{\circ\prime}_{2-/3-}$	Compound	$E^{\circ\prime}_{2-/3-}$
$[Fe(WS_4)_2]^{2-}$	−0.72	–	–	–	
$[Co(MoS_4)_2]^{2-}$	−0.82	$[Co(MoOS_3)_2]^{2-}$	−0.90	$[Co(MoO_2S_2)_2]^{2-}$	−1.23
$[Co(WS_4)_2]^{2-}$	−1.00	$[Co(WOS_3)_2]^{2-}$	−1.07	$[Co(WO_2S_2)_2]^{2-}$	−1.29
$[Ni(MoS_4)_2]^{2-}$	−1.06	$[Ni(MoOS_3)_2]^{2-}$	−1.13	$[Ni(MoO_2S_2)_2]^{2-}$	−1.17
$[Ni(WS_4)_2]^{2-}$	−1.06	$[Ni(WOS_3)_2]^{2-}$	−1.13	$[Ni(WO_2S_2)_2]^{2-}$	−1.23

similar to that experienced by $[Cu_2Cl_2WS_4]^{2-}$ [93].

(xi) Molybdenum–ruthenium clusters

(a) $MoRu_2S_4$ core

The structure reported in Fig. 39 has been assigned to $[(C_5H_5)Ru(PPh_3)]_2MoS_4$ [96]. It is briefly reported that in dichloromethane this thiomolybdate compound undergoes a reversible one-electron oxidation process at −0.06 V [96]. The probable stable monocation has not so far been characterized.

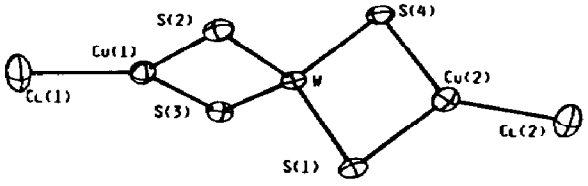

Fig. 37. Crystal structure of $[Cu_2Cl_2WS_4]^{2-}$. Selected mean distances within the Cu_2WS_4 core: W–S 2.21 Å, Cu–S 2.40 Å, Cu–W 2.62 Å (from ref. 93).

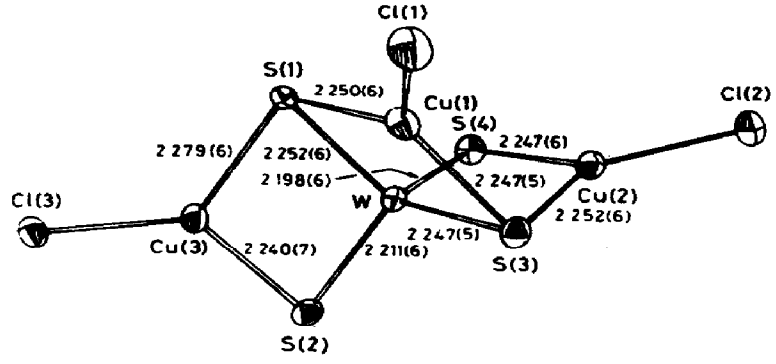

Fig. 38. Perspective view of $[Cu_3Cl_3WS_4]^{2-}$ (with selected mean distances) (from ref. 94).

TABLE 15

Redox potentials (in volts) for the reduction processes of $[Pd(MoS_4)_2]^{2-}$

$E^{\circ\prime}_{2-/3-}$	$E^{\circ\prime}_{3-/4-}$	Solvent	Ref.
−1.41	−1.72	AN [a]	87
−1.54	−1.78	DMF	87
−1.06	–	DCM	89

[a] $(C_3H_7)_4NBr$ supporting electrolyte.

(xii) Molybdenum–palladium clusters

(a) $PdMo_2S_8$ core

The $[Pd(MoS_4)_2]^{2-}$ dianion is isostructural with $[Ni(MoS_4)_2]^{2-}$, whose structure is reported in Fig. 32. As shown in Fig. 40, $[Pd(MoS_4)_2]^{2-}$ undergoes two sequential one-electron cathodic processes [87,88].

In contrast with the nickel analogue, which gives rise to two distinct reversible steps, in the present case the two processes are very close to each other, with only the first being fully reversible (Table 15). Whereas the electrogeneratable tetra-anion is totally unstable, the relevant trianion has been spectroscopically characterized [89].

The shift of the $2-/3-$ step towards more negative potential values and the closeness of the $2-/3-$ and $3-/4-$ steps, in comparison with the corresponding nickel complex, is attributed to the fact that the increase in

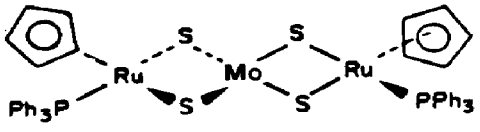

Fig. 39. Proposed structure for $[(C_5H_5)_2Ru_2(PPh_3)_2]MoS_4$.

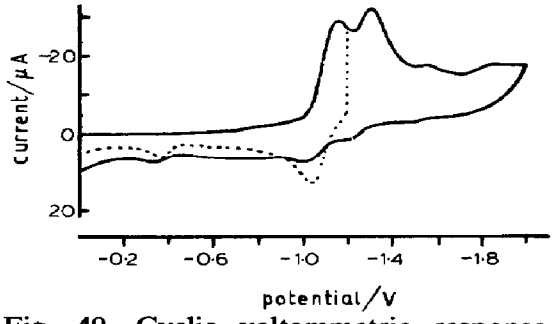

Fig. 40. Cyclic voltammetric response recorded in a dimethylformamide solution of $[Pd(MoS_4)_2]^{2-}$. Potential values vs. SCE (from ref. 88).

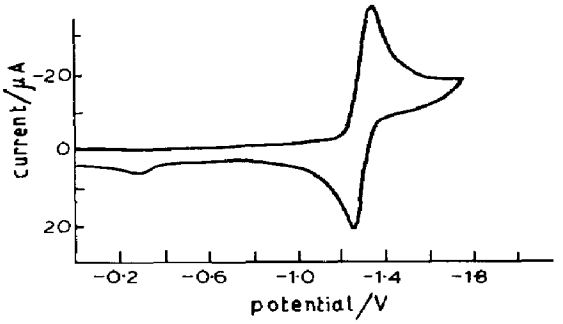

Fig. 41. Cyclic voltammogram recorded in a dimethylformamide solution of $[Pt(MoS_4)_2]^{2-}$. Potential values vs. SCE (from ref. 88).

the mass of the central atom causes both the a_g (Pd-centered) and the b_{1g} (ligand-centered) molecular orbitals to rise in energy, while becoming very close to each other, so that the first electron enters the Pd level, while the second electron enters the ligand level (probably because of an a_g–b_{1g} energy separation lower than the pairing energy in a_g) [87].

(xiii) Molybdenum–platinum clusters

(a) $PtMo_2S_8$ core

The dianion $[Pt(MoS_4)_2]^{2-}$, isostructural with $[Ni(MoS_4)_2]^{2-}$ and $[Pd(MoS_4)_2]^{2-}$, undergoes, at variance with these analogues, a single reversible two-electron reduction process (Fig. 41) (Table 16 [87,88]).

The extent of the electrochemical reversibility of the two coincident, or nearly coincident, one-electron steps was difficult to ascertain being dependent both upon the solvent and the supporting electrolyte.

The occurrence of two overlapping one-electron steps, at potentials more negative than those of the nickel and palladium analogues, agrees with a further mass-dependent lowering of the ligand-centered b_{1g} orbital to the energy of the Pt-centered a_g orbital, and their consequent half filling [87].

TABLE 16

Redox potential (in volts) for the two-electron reduction process of $[Pt(MoS_4)_2]^{2-}$ [87]

$E^{o\prime}_{2-/4-}$	Solvent
−1.64	AN [a]
−1.79	DMF [a]

[a] $(C_3H_7)_4NBr$ supporting electrolyte.

(xiv) Tungsten–ruthenium clusters

(a) WRu_2S_4 core

The series of derivatives shown in Scheme 15, which contains the linear assembly WRu_2S_4, isostructural with the $MoRu_2S_4$ core considered in Section B (xi) (a) has been characterized [96].

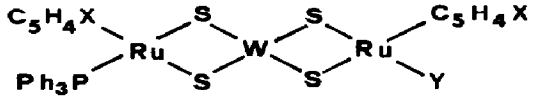

X = H, CH_3
Y = PPh_3, CO

Scheme 15

Like the corresponding thiomolybdates, these derivatives undergo a reversible one-electron anodic process in dichloromethane (Table 17).

The ligand effects upon the electrode potentials are quite expected. The substitution of a π-accepting CO group with a σ-donating PPh_3 group, as well as the presence of an electron donating methyl substituent in the cyclopentadienyl moiety facilitates oxidation to the monocation.

Data on the one-electron oxidized species have not yet appeared.

(xv) Tungsten–palladium clusters

(a) PdW_2S_8 core

In the preceding sections (namely Sections B (viii) (a) and B (ix) (a)) it was reported that $[Ni(MoS_4)_2]^{2-}$ and $[Ni(WS_4)_2]^{2-}$ undergo qualitatively similar redox changes. The same behavior holds for $[Pd(WS_4)_2]^{2-}$ and $[Pd(MoS_4)_2]^{2-}$. In fact, by analogy with $[Pd(MoS_4)_2]^{2-}$, $[Pd(WS_4)_2]^{2-}$ undergoes two sequential closely spaced one-electron reduction processes (the first one reversibly, the second irreversibly) (Table 18). Proposed rationalizations for this redox behavior have been presented in Section B (xii) (a).

TABLE 17

Formal electrode potentials (in volts) for the one-electron anodic step of $[(C_5H_4X)_2Ru_2(PPh_3)Y]WS_4$ in dichloromethane [96]

X	Y	$E^{\circ\prime}_{0/1+}$
H	PPh_3	+0.05
H	CO	+0.19
CH_3	PPh_3	−0.06
CH_3	CO	+0.90

TABLE 18

Redox potentials (in volts) for the reduction processes of $[Pd(WS_4)_2]^{2-}$

$E^{o'}_{2-/3-}$	$E_{p3-/4-}$	Solvent	Ref.
−1.41	−1.85	AN [a]	87
−1.51	−1.91	DMF [a]	87
−1.14	–	DCM	89

[a] $(C_3H_7)_4NBr$ supporting electrolyte.

TABLE 19

Redox potential (in volts) for the reduction process of $[Pt(WS_4)_2]^{2-}$ [87]

$E^{o'}_{2-/4-}$	Solvent
−1.67	AN [a]
−1.80	DMF [a]

[a] $(C_2H_5)_4NClO_4$ supporting electrolyte.

The electrogenerated trianion $[Pd(WS_4)_2]^{3-}$ has been characterized by ESR techniques [89].

(xvi) Tungsten–platinum clusters

(a) PtW_2S_8 core

The dianion $[Pt(WS_4)_2]^{2-}$ behaves in the same manner as $[Pt(MoS_4)_2]^{2-}$, giving rise to a single two-electron reduction step [87,88] (Table 19). Plausible explanations for these redox properties have been presented in Section B (xii) (a).

C. HETEROTRIMETALLIC SULFUR CLUSTERS

Very few polynuclear derivatives containing three different metal species have been examined electrochemically, and up to now all of them belong to the triangular species capped by a triply bridging sulfur atom, as illustrated in Scheme 16.

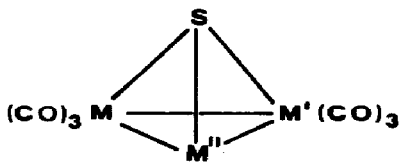

Scheme 16

(i) Iron–cobalt–molybdenum clusters

(a) FeCoMoS core

The carbonyl complex $(\mu_3\text{-S})FeCoMo(C_5H_5)(CO)_8$ has a structure similar to that reported in Scheme 16 (M = Fe, M′ = Co, M″ = Mo) [97].

In dichloroethane this cluster undergoes a quasi-reversible one-electron reduction process at $E^{\circ\prime} = -1.60$ V, and a declustering oxidation process at $E_p = +0.65$ V [14].

Comparison with the isostructural $(\mu_3\text{-S})FeCo_2(CO)_9$ (Section B (i) (a)) indicates that in the present case access to the monoanion species is notably more difficult ($\Delta E^{\circ\prime} \sim 0.5$ V). This result can be ascribed to two sources: (i) the presence of a Mo atom heavier than a Co atom; (ii) the substitution of one acceptor carbonyl molecule by an electron-donating cyclopentadienyl molecule.

(ii) Iron–cobalt–tungsten clusters

(a) FeCoWS core

The complex $(\mu_3\text{-S})FeCoW(C_5H_5)(CO)_8$ is isostructural with $SFeCoMo(C_5H_5)(CO)_8$, cited previously [97]. In dichloroethane it undergoes a quasi-reversible one-electron reduction process at $E^{\circ\prime} = -1.79$ V, and a declustering oxidation process at $E_p = +0.55$ V [14].

The shift of the $0/1-$ couple towards more negative potentials (by about 0.2 V), in comparison with the corresponding FeCoMo analogue, must be attributed to the presence of W which is heavier than Mo.

(iii) Cobalt–molybdenum–ruthenium clusters

(a) CoMoRuS core

The complex $(\mu_3\text{-S})CoMoRu(C_5H_5)(CO)_8$ has the geometry illustrated in Scheme 16 (M = Co, M′ = Ru, M″ = Mo) [85]. As in previous cases, in dichloroethane, it undergoes a quasi-reversible one-electron reduction step (at $E^{\circ\prime} = -1.75$ V) and an irreversible oxidation process ($E_p = +0.45$ V) [14].

Once again the different nature of the trimetal moiety explains the difference in the redox potential of the $0/1-$ couple in comparison with the FeCoMo analogue.

In conclusion, these redox data for heterotrimetallic species together with those reported in Section B (i) confirm that in trimetallic $(\mu_3\text{-S})$–carbonyl complexes the LUMO is essentially metal based, and conjugated to the in-plane ligands.

D. APPENDIX

Just after the submission of the present review a pertinent paper dealing with the structure and redox behavior of a series of heterodimetal–sulfur clusters appeared [98].

Figure 42 shows the molecular structure of $(CH_3C_5H_4)_2Mo_2S_4Fe_2(CO)_6$: The centrosymmetric $Fe_2Mo_2S_4$ core consists of a planar array of the four metal ions (two Mo(III) and two Fe(II) centers) bridged by four triply bridging sulfur atoms, which in turn lie in a plane perpendicular to the metallic plane.

In cyclic voltammetry, in acetonitrile, this complex displays two declustering oxidation processes and two one-electron reductions ($E^{\circ\prime} = -1.50$ V and -1.78 V respectively), probably centered on the successive redox changes Mo(III)Mo(III)/Mo(III)Mo(II) and Mo(III)Mo(II)/Mo(II)Mo(II), complicated by subsequent chemical reactions ($i_{pa}/i_{pc} \neq 1$) [98]. Accordingly, the use of reducing agents afforded the desulfurized complex $(CH_3C_5H_4)_2Mo_2S_3Fe_2(CO)_6$ (described as a Mo(II)Mo(II) dimer with two Fe(II) units), the structure of which is reported in Fig. 43. In this centrosymmetric $Mo_2Fe_2S_3$ core there are two triply bridging and one quadruply bridging sulfido ligands. Both the iron and sulfur atoms form a plane perpendicular to the Mo–Mo axis.

With respect to the parent $Mo_2Fe_2S_4$ core, the desulfurizing addition of two electrons causes a significant elongation of the Mo–Mo distance (-0.05 Å), as well as an equivalent shortening of both the Mo–Fe and Mo–μ_3S distances, while leaving the Fe–μ_3S bond constant.

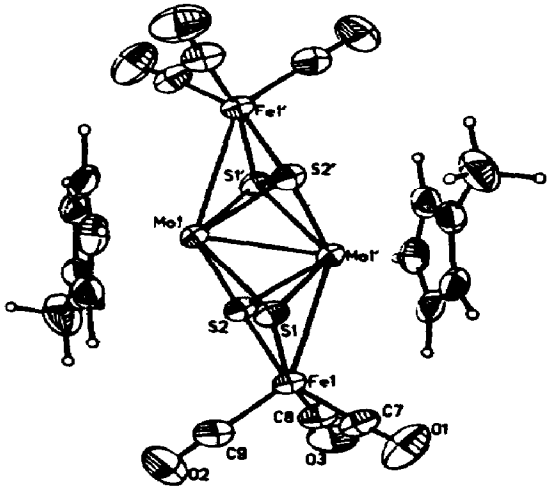

Fig. 42. Crystal structure of $[(CH_3C_5H_4)MoS_2Fe(CO)_3]_2$. Core mean distances: Mo–Mo 2.62 Å; Mo–Fe 2.85 Å; Mo–μ_3S 2.43 Å; Fe–μ_3S 2.23 Å (from ref. 98).

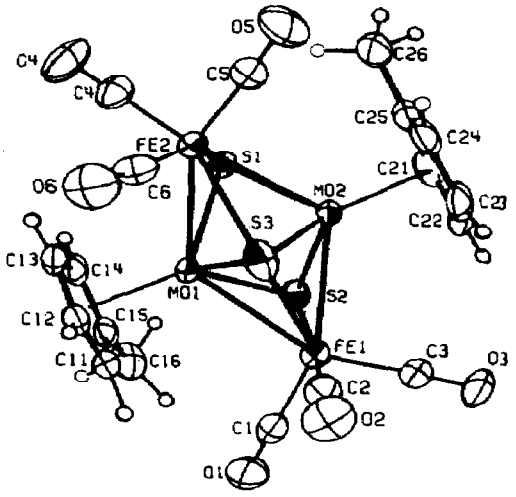

Fig. 43. Molecular structure of $(CH_3C_5H_4)_2Mo_2S_3Fe_2(CO)_6$. Core mean distances: Mo–Mo 2.67 Å; Mo–Fe 2.80 Å; Mo–μ_3S 2.38 Å; Fe–μ_3S 2.23 Å; Mo–μ_4S 2.31 Å; Fe–μ_4S 2.55 Å (from ref. 98).

Figure 44 shows the cyclic voltammetric behavior of $(CH_3C_5H_4)_2Mo_2S_3Fe_2(CO)_6$. A two-electron quasi-reversible uncomplicated reduction process ($E^{\circ\prime} = -1.38$ V) precedes an uncomplicated one-electron quasi-reversible cathodic step ($E^{\circ\prime} = -1.97$ V). Neither the assignment of these charge transfers, nor the characterization of the probable stable reduction products have been performed.

The two isoelectronic complexes $[(CH_3C_5H_4)_2Mo_2S_4Fe(C_5H_5)]^+$ and $[(CH_3C_5H_4)_2Mo_2S_4Co(C_5H_5)]^{2+}$ have also been characterized [98].

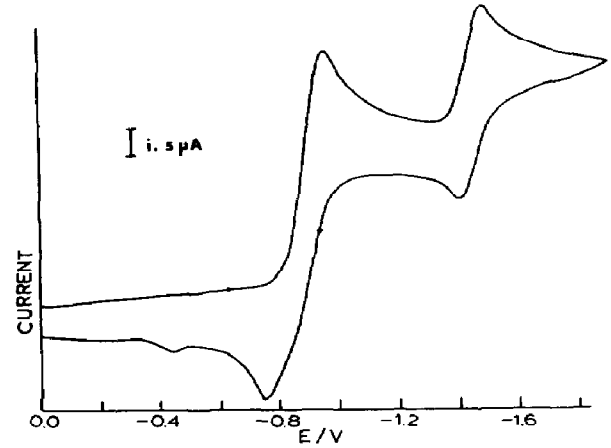

Fig. 44. Cyclic voltammogram recorded at a platinum electrode on an acetonitrile solution of $(CH_3C_5H_4)_2Mo_2S_3Fe_2(CO)_6$. Potential values vs. SCE (from ref. 98).

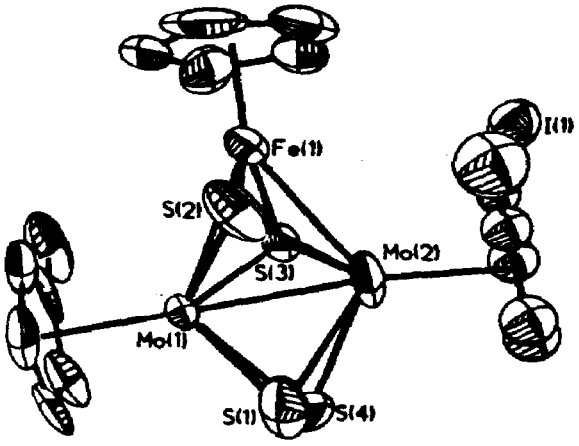

Fig. 45. Crystal structure of $[(CH_3C_5H_4)_2Mo_2S_4Fe(C_5H_5)]^+$. Core mean distances: Mo–Mo 2.60 Å; Mo–Fe 2.78 Å; Mo–μ_3S 2.38 Å; Fe–μ_3S 2.13 Å; Mo–$\mu_2\eta^2$S 2.45 Å (from ref. 98).

Figure 45 illustrates the structure of the $FeMo_2S_4$ derivative. It consists of a closed triangle of metal ions bicapped by triply bridging sulfur atoms above and below the trimetallic plane. In addition the two molybdenum ions are also bridged to a disulfido ligand.

The redox activity of this compound in acetonitrile shows an irreversible reduction process ($E_p = -1.26$ V), and two quasi-reversible oxidation processes ($E^{\circ\prime} = -0.15$ V and $E^{\circ\prime} = +0.26$ V respectively).

The probable isostructural $CoMo_2S_4$ derivative exhibits three quasi-reversible reduction processes ($E^{\circ\prime} = -0.50$ V, $E^{\circ\prime} = -0.94$ V and $E^{\circ\prime} = -1.18$ V respectively) of which only the less cathodic is uncomplicated by coupled chemical reactions. There are two quasi-reversible anodic processes ($E^{\circ\prime} = -0.17$ V and $E^{\circ\prime} = +0.23$ V respectively).

In both complexes, the anodic processes are attributed to the oxidation of the iodide counteranion. In the case of the cobalt complex the reduction processes are attributed to the sequential redox changes Co(III)/Co(II), Co(II)/Co(I) and Co(I)/Co(0), whereas in the case of the iron complex they are attributed to the usually irreversible Fe(II)/Fe(I) step [98].

E. CONCLUSION

The chemistry of heterometallic sulfur clusters is relatively younger than that of homometallic sulfur clusters, and this is reflected in the smaller number of studies devoted to their redox behavior.

One of the aims of this review, which emphasizes those clusters whose redox chemistry has been elucidated and gives evidence of chemically reversible redox changes which have not yet been fully exploited from the

preparative and/or structural viewpoint, is to encourage research in this area in order to throw light on the stereochemical consequences of the electron addition to or removal from polynuclear cores. In fact, from the evidence of the pioneering work of Dahl and coworkers, this aspect is of considerable importance to the bonding description of such compounds, which is generally less well developed than those of mononuclear or dinuclear species.

REFERENCES

1 R.H. Holm, Chem. Soc. Rev., 10 (1981) 455.
2 D. Coucouvanis, Acc. Chem. Res., 14 (1981) 201.
3 B.A. Averill, Struct. Bonding (Berlin), 53 (1983) 59.
4 W.E. Newton, F.A. Schultz, S.F. Gheller, S. Lough, J.W. McDonald, S.D. Conradson, B. Hedman and K.O. Hodgson, Polyhedron, 5 (1986) 567.
5 R.L. Robson, R.R. Eady, T.H. Richardson, R.W. Miller, M. Hawkins and J.R. Postgate, Nature (London), 322 (1986) 388.
6 B.J. Hales, E.E. Case, J.E. Morningstar, M.F. Dzeda and L.A. Mauterer, Biochemistry, 25 (1986) 7251.
7 R.R. Eady, R.L. Robson, B.E. Smith, D.J. Lowe, R.W. Miller and M.J. Dilworth, Recl. Trav. Chim. Pays-Bas, 106 (1987) 175.
8 I. Moura, J.J.G. Moura, E. Münck, V. Papaefthymiou and J. Le Gall, J. Am. Chem. Soc., 108 (1986) 349.
9 K.K. Surerus, E. Münich, I. Moura, J.J.G. Moura and J. Le Gall, J. Am. Chem. Soc., 109 (1987) 3805.
10 N.A. Vaute, W. Jaegermann, H. Tributsch, W. Hönle and K. Yvon, J. Am. Chem. Soc., 109 (1987) 3251.
11 P. Zanello, Coord. Chem. Rev., 83 (1988) 199.
12 D.L. Stevenson, C.H. Wei and L.F. Dahl, J. Am. Chem. Soc., 93 (1971) 6027.
13 B.M. Peake, P.H. Rieger, B.H. Robinson and J. Simpson, Inorg. Chem., 20 (1981) 2540.
14 U. Honrath and H. Vahrenkamp, Z. Naturforsch., Teil B, 39 (1984) 545.
15 L. Markò, J. Organomet. Chem., 213 (1981) 271.
16 P.L. Dahlstron, S. Kumar and J. Zubieta, J. Chem. Soc., Chem. Commun., (1981) 411.
17 J.W. McDonald, G.D. Friesen and W.E. Newton, Inorg. Chim. Acta, 46 (1980) L79.
18 D. Coucouvanis, E.D. Simhon and N.C. Baenziger, J. Am. Chem. Soc., 102 (1980) 6644.
19 G.A. Bowmaker, P.D.W. Boyd, R.J. Sorreson, C.A. Reed and J.W. McDonald, Inorg. Chem., 26 (1987) 3.
20 A. Müller and S. Sarkar, Angew. Chem. Int. Ed. Engl., 16 (1977) 705.
21 D. Coucouvanis, N.C. Baenziger, E.D. Simhon, P. Stremple, D. Swenson, A. Simopoulos, A. Kostikas, V. Petrouleas and V. Papaefthymiou, J. Am. Chem. Soc., 102 (1980) 1732.
22 D. Coucouvanis, E.D. Simhon, P. Stremple, M. Ryan, D. Swenson, N.C. Baenziger, A. Simopoulos, V. Papaefthymiou, A. Kostikas and V. Petrouleas, Inorg. Chem., 23 (1984) 741.
23 R.H. Tieckelmann and B.A. Averill, Inorg. Chim. Acta, 46 (1980) L35.
24 R.E. Palermo, R. Singh, J.K. Bashkin and R.H. Holm, J. Am. Chem. Soc., 106 (1984) 2600.
25 W.H. Armstrong, P.K. Mascharak and R.H. Holm, Inorg. Chem., 21 (1982) 1699.
26 W.H. Armstrong, P.K. Mascharak and R.H. Holm, J. Am. Chem. Soc., 104 (1982) 4373.

27 P.K. Mascharak, W.H. Armstrong, Y. Mizobe and R.H. Holm, J. Am. Chem. Soc., 105 (1983) 475.
28 Y. Mizobe, P.K. Mascharak, R.E. Palermo and R.H. Holm, Inorg. Chim. Acta, 80 (1983) L65.
29 R.E Palermo and R.H. Holm, J. Am. Chem. Soc., 105 (1983) 4310.
30 Y.-P. Zhang, J.K. Bashkin and R.H. Holm, Inorg. Chem., 26 (1987) 694.
31 T.E. Wolff, J.M. Berg and R.H. Holm, Inorg. Chem., 20 (1981) 174.
32 H.C. Silvis, R.H. Tieckelmann and B.A. Averill, Inorg. Chim. Acta, 36 (1979) L423.
33 D. Coucouvanis and M.G. Kanatzidis, J. Am. Chem. Soc., 107 (1985) 5005.
34 M.G. Kanatzidis and D. Coucouvanis, J. Am. Chem. Soc., 108 (1986) 337.
35 A. Salifoglou, M.G. Kanatzidis and D. Coucouvanis, J. Chem. Soc., Chem. Commun., (1986) 559.
36 D. Coucouvanis, A. Salifoglou, M.G. Kanatzidis, A. Simopoulos and A. Kostikas, J. Am. Chem. Soc., 109 (1987) 3807.
37 G. Christou, C.D. Garner and F.E. Mabbs, J. Chem. Soc., Chem. Commun., (1978) 740.
38 G. Christou, C.D. Garner, F.E. Mabbs and M.G.B. Drew, J. Chem. Soc., Chem. Commun., (1979) 91.
39 T.E. Wolff, J.M. Berg, K.O. Hodgson, R.B. Frankel and R.H. Holm, J. Am. Chem. Soc., 101 (1979) 4140.
40 G. Christou, C.D. Garner, R.M. Miller, C.E. Johnson and J.D. Rush, J. Chem. Soc., Dalton Trans., (1980) 2363.
41 G. Christou, C.D. Garner and F.E. Mabbs, Inorg. Chim. Acta, 29 (1978) L189.
42 T.E. Wolff, P.P. Power, R.B. Frankel and R.H. Holm, J. Am. Chem. Soc., 102 (1980) 4694.
43 R.R. Gagné, C.A. Koval, T.J. Smith and M.C. Cimolino, J. Am. Chem. Soc., 101 (1979) 4571.
44 T.E. Wolff, J.M. Berg, P.P. Power, K.O. Hodgson, R.H. Holm and R.B. Frankel, J. Am. Chem. Soc., 101 (1979) 5454.
45 G. Christou, P.K. Mascharak, W.H. Armstrong, G.C. Papaefthymiou, R.B. Frankel and R.H. Holm, J. Am. Chem. Soc., 104 (1982) 2820.
46 G. Christou, C.D. Garner and R.M. Miller, J. Inorg. Biochem., 11 (1979) 349.
47 S.R. Acott, G. Christou, C.D. Garner, T.J. King, F.E. Mabbs and R.M. Miller, Inorg. Chim. Acta, 35 (1979) L337.
48 R.E. Palermo, P.P. Power and R.H. Holm, Inorg. Chem., 21 (1982) 173.
49 W.E. Cleland, Jr., and B.A. Averill, Inorg. Chim. Acta, 107 (1985) 187.
50 K. Tanaka, M. Moriya and T. Tanaka, Inorg. Chem., 25 (1986) 835.
51 G. Christou, R.V. Hageman and R.H. Holm, J. Am. Chem. Soc., 102 (1980) 7600.
52 S. Kuwabata, K. Tanaka and T. Tanaka, Inorg. Chem., 25 (1986) 1691.
53 S. Kuwabata, S. Uezumi, K. Tanaka and T. Tanaka, Inorg. Chem., 25 (1986) 3018.
54 G. Christou, C.D. Garner, T.J. King, C.E. Johnson and J.D. Rush, J. Chem. Soc., Chem. Commun., (1979) 503.
55 G. Christou and C.D. Garner, J. Chem. Soc., Dalton Trans., (1980) 2354.
56 T.E. Wolff, J.M. Berg, C. Warrick, K.O. Hodgson, R.H. Holm and R.B. Frankel, J. Am. Chem. Soc., 100 (1978) 4630.
57 J.A. Kovacs, J.K. Bashkin and R.H. Holm, J. Am. Chem. Soc., 107 (1985) 1784.
58 T.E. Wolff, J.M. Berg, P.P. Power, K.O. Hodgson and R.H. Holm, Inorg. Chem., 19 (1980) 430.
59 P. Stremple, N.C. Baenziger and D. Coucouvanis, J. Am. Chem. Soc., 103 (1981) 4601.
60 A. Müller, W. Hellmann, C. Römer, M. Römer, H. Bögge, R. Jostes and U. Schimanski, Inorg. Chim. Acta, 83 (1984) L75.

61 A. Müller, E. Diemann, R. Jostes and H. Bögge, Angew. Chem. Int. Ed. Engl., 20 (1981) 934.
62 J.W. McDonald, G.D. Friesen, W.E. Newton, A. Müller, W. Hellmann, U. Schimanski, A. Trautwein and U. Bender, Inorg. Chim. Acta, 76 (1983) L297.
63 G.D. Friesen, J.W. McDonald, W.E. Newton, W.B. Euler and B.M. Hoffman, Inorg. Chem., 22 (1983) 2202.
64 C.D. Garner and R.M. Miller, J. Chem. Soc., Dalton Trans., (1981) 1664.
65 Y. Do, E.D. Simhon and R.H. Holm, J. Am. Chem. Soc., 105 (1983) 6731.
66 Y. Do, E.D. Simhon and R.H. Holm, Inorg. Chem., 24 (1985) 4635.
67 C.M. Bolinger, T.B. Rauchfuss and S.R. Wilson, J. Am. Chem. Soc., 104 (1982) 7313.
68 C.M. Bolinger, T.D. Weatherwill, T.B. Rauchfuss, A.L. Rheingold, C.S. Day and S.R. Wilson, Inorg. Chem., 25 (1986) 634.
69 T.B. Rauchfuss, T.D. Weatherill, S.R. Wilson and J.P. Zebrowski, J. Am. Chem. Soc., 105 (1983) 6508.
70 J.A. Kovacs and R.H. Holm, J. Am. Chem. Soc., 108 (1986) 340.
71 J.A. Kovacs and R.H. Holm, J. Am. Chem. Soc., 108 (1986) 1342.
72 J.A. Kovacs and R.H. Holm, Inorg. Chem., 26 (1987) 702.
73 J.A. Kovacs and R.H. Holm, Inorg. Chem., 26 (1987) 711.
74 M.J. Carney, J.A. Kovacs, Y.-P. Zhang, G.C. Papaefthymiou, K. Spartalian, R.B. Frankel and R.H. Holm, Inorg. Chem., 26 (1987) 719.
75 A. Müller, R. Jostes, W. Hellmann, C. Römer, H. Bögge and U. Schimanski, Z. Anorg. Allg. Chem., 533 (1986) 125.
76 L. Szterenberg and B. Jezowska-Trzebiatowska, Inorg. Chim. Acta, 86 (1984) L29.
77 E. Königer-Ahlborn and A. Müller, Angew. Chem. Int. Ed. Engl., 13 (1974) 672.
78 A. Müller, E. Königer-Ahlborn, E. Krickemeyer and R. Jostes, Z. Anorg. Allg. Chem., 483 (1981) 69.
79 A. Müller, N. Mohan and H. Bögge, Z. Naturforsch. Teil B, 33 (1978) 978.
80 A. Müller, R. Jostes, V. Flemming and R. Potthast, Inorg. Chim. Acta, 44 (1980) L33.
81 A. Müller, W. Hellman, J. Schneider, U. Schimanski, U. Demmer, A. Trautwein and U. Bender, Inorg. Chim. Acta, 65 (1982) L41.
82 A. Müller, W. Hellman and W.E. Newton, Z. Naturforsch. Teil B, 38 (1983) 528.
83 A. Müller and H.-H. Heinsen, Chem. Ber., 105 (1972) 1730.
84 A. Müller, H.-H. Heinsen and G. Vandrish, Inorg. Chem., 13 (1974) 1001.
85 E. Roland and H. Vahrenkamp, Chem. Ber., 117 (1984) 1039.
86 I. Sotofte, Acta Chem. Scand. Ser. A, 30 (1976) 157.
87 K.P. Callahan and P.A. Piliero, Inorg. Chem., 19 (1980) 2619.
88 K.P. Callahan and P.A. Piliero, J. Chem. Soc., Chem. Commun., (1979) 13.
89 G.A. Bowmaker, P.D.W. Boyd, G.K. Campbell and M. Zvagulis, J. Chem. Soc., Dalton Trans., (1986) 1065.
90 A. Müller and E. Diemann, J. Chem. Soc., Chem. Commun., (1971) 65.
91 A. Müller, E. Diemann and H.-H. Heinsen, Chem. Ber., 104 (1971) 975.
92 A. Müller, H. Bögge, E. Krickemeyer, G. Henkel and B. Krebs, Z. Naturforsch. Teil B, 37 (1982) 1014.
93 F. Sécheresse, M. Salis, C. Potvin and J.-M. Manoli, Inorg. Chim. Acta, 114 (1986) L19.
94 J.-M. Manoli, C. Potvin and F. Sécheresse, J. Chem. Soc., Chem. Commun., (1982) 1159.
95 C. Potvin, J.-M. Manoli, M. Salis and F. Sécheresse, Inorg. Chim. Acta, 83 (1984) L19.
96 K.E. Howard, T.B. Rauchfuss and A.L. Rheingold, J. Am. Chem. Soc., 108 (1986) 297.
97 F. Richter and H. Vahrenkamp, Chem. Ber., 115 (1982) 3224.
98 B.A. Cowans, R.C. Haltiwanger and M.R. DuBois, Organometallics, 6 (1987) 995.